Validation of GRACE-derived terrestrial water storage from a regional approach over South America

Frédéric Frappart, Lucia Seoane, Guillaume Ramillien

Validation of GRACE-derived Terrestrial Water Storage from a regional approach over South America

Frédéric Frappart (1,2), Lucía Seoane (1), Guillaume Ramillien (1,2)

(1) Université de Toulouse, OMP-GET, UM5563, CNRS/IRD/UPS, 14 Avenue Edouard Belin, 31400 Toulouse, France
(2) Groupe de Recherche en Géodésie Spatiale

Abstract : We propose to validate regional solutions consisting of 2° surface tiles of surface mass concentration over South America (90°W-30°W; 60°S-20°N) computed using accurate Level-1 GRACE measurements, by confronting them to other GRACE products (i.e., global GRGS and ICA-400 km GFZ/CSR/JPL combined solutions) and independent *in situ* river level and discharge datasets. For this purpose, Principal Component Analysis (PCA) was applied to all these types of the GRACE-based solutions to extract the corresponding main orthogonal spatial and temporal modes of variability to be compared for 2003-2010. For the first three spatial modes, regional solutions provide a better geographical localization of hydrological structures, especially indicating major surface and groundwater systems of South America. Over hydrological patterns, records of river level versus time are particularly consistent with the GRACE temporal modes, especially for our regional solutions (*i.e.*, correlations generally greater than 0.7). Interannual variations of GRACE-based Terrestrial Water Storage (TWS) clearly exhibit the signatures of extreme climatic events as the recent droughts and floods that affected South America. Very significant agreement is also found at interannual time-scale between TWS and discharges in drainage basins dominated by the surface reservoir (more than 0.9 of correlation in the Amazon basin).

Keywords : GRACE; surface water; groundwater, water levels; discharges

1. Introduction

Continental water storage is a key component of the global hydrological cycle which plays a major role in the Earth's climate system that controls over water, energy and biogeochemical fluxes. In spite of its importance, the total continental water storage is not well-known at regional and global scales because of the disparity of *in situ* observations and systematic monitoring of the terrestrial water reservoirs, especially the groundwater component (Alsdorf and Lettenmaier, 2003).

The Gravity Recovery and Climate Experiment (GRACE) mission provides a global mapping of the time-variations of the gravity field at an unprecedented resolution of ~400 km and a centimetric precision in terms of geoid height. Tiny variations of gravity measured by GRACE are mainly due to redistribution of mass inside the fluid envelops of the Earth (*i.e.*, atmosphere, oceans and continental water storage) from monthly to decadal timescales (Tapley et al., 2004).

Since its launch in March 2002, the GRACE terrestrial water storage anomalies have been increasingly used for large-scale hydrological applications (see Ramillien et al., 2008a; Schmidt et al., 2008 for reviews). These studies demonstrated a great potential to monitor extreme hydrological events (Andersen et al., 2005; Seitz et al., 2008; Chen et al., 2009; Frappart et al., in press), to monitor aquifer storage (Rodell et al., 2007; Strassberg et al., 2007; Leblanc et al., 2009) and snowpack (Frappart et al., 2011a) variations, and to estimate hydrological fluxes, such as basin-scale evapotranspiration rate (Rodell et al., 2004; Ramillien et al. , 2006) and discharge (Syed et al., 2009).

Unfortunately, GRACE Level-2 solutions suffer from the presence of important north-south striping when determining Stokes coefficients (*i.e.*, spherical harmonics of the geopotential

corrected from known gravitational accelerations using *a priori* models for atmosphere, ocean mass, and tides) which are geophysically unrealistic, and aliasing of short-time phenomena. Because of these effects of striping that limits further interpretation, different post-processing approaches for filtering these residual GRACE geoid solutions have been proposed to extract useful hydrological signals (see Ramillien et al., 2008a; Schmidt et al., 2008 for reviews) with the risk of losing energy in the short wavelengths domain, and thus missing details (*i.e.*, loss of resolution).

To overcome this problem, local determination of the time variations of the surface water storage has been developed (Rowlands et al., 2005; Eicker, 2008). They are of great interest for regions where very localized important mass variations occur, such as flood and glaciers fields. Mascons consist of adjusting regional heights of individual surface elements by using scaling factors of spherical harmonics. However, they remain equivalent to classical global solutions (Rowlands et al., 2010). Another type of regional approach has been more recently proposed by directly adjusting the surface mass density distribution at the surface of the Earth from the Level-1 GRACE data, especially the accurate satellite-to-satellite velocity variations or K-Band Range Rate (KBRR) measurements (Ramillien et al., 2011), and taking spatial correlations versus the geographical distance between juxtaposed surface elements into account (Ramillien et al., 2012).

In particular, power spectral density reveals that the regional solutions computed over South America are more energetic than the bandlimited global Level-2 solutions at short and medium spatial wavelengths (<4,000 km) (Ramillien et al., 2012). In the present study, our goal is to demonstrate that the excess of energy present at short wavelengths (between 400 and 1000 km) in the regional solutions compared to the global solutions can be related to realistic geophysical signals corresponding to hydrological events such as floods, melt of glaciers, or groundwater variations. To verify this assumption, a Principal Component Analysis (PCA) was first applied to

the GRACE-based regional and global solutions. The resulting spatial and temporal modes were compared to spatial distribution of surface and ground waters and correlated to water levels variations from *in situ* gauges located close to the mouth of the major river basins and sub-basins of South America respectively. Then, basin-averaged anomalies of TWS from this regional approach are compared with changes of *in situ* surface water discharges in the largest drainage basins of South America (*i.e.*, Amazon, La Plata, Orinoco, and Tocantins), as well as basin-averaged anomalies of TWS from global GRACE solutions.

To our knowledge, there is no large area in the world covered with a sufficient density of *in situ* measurements of all the hydrological reservoirs to directly validate GRACE data. Most of the previous studies dealing with the validation of the data present comparisons between GRACE-based TWS and hydrological outputs, and/or comparisons with external hydrological datasets such as gridded rainfall and *in situ* water levels and discharges (see Ramillien et al., 2008a; Schmidt et al., 2008 for reviews). Here, we have chosen to compare the GRACE-based TWS from our regional approach to other global available solutions and to, according to your opinion, a profound and extensive datasets of in situ water levels. We decided not to compare to hydrological model outputs because most of the hydrological models do not simulate the slow reservoirs such as the floodplains and the groundwater.

2. Datasets & Methods

2.1 Water mass variations from GRACE solutions

2.1.1 Constrained regional solutions

An alternative regional approach to the ones based on spherical harmonics has been recently proposed to improve geographical localization of hydrological structures and to reduce leakage

and aliasing errors. Our regional approach consists of determining water mass variations over juxtaposed surface elements in a given continental region from GRACE residuals potential differences anomalies, in terms of equivalent-water heights. According to the energy integral approach, these latter along-track anomalies correspond mainly to the contribution of the continental hydrology to the gravity field changes measured by GRACE, they are obtained from KBR range velocities differences between the two GRACE satellites after a priori (*i.e.,* de-aliasing) corrections of mass variations ocurring in the oceans and the atmosphere, are made by pre-processing of GRACE observations. By assuming the conservation of energy along the GRACE groundtracks, it consists of recovering equivalent-water thicknesses of juxtaposed 2 by 2-degree geographical tiles by inverting GRACE inter-satellite KBR Range (KBRR) residuals (see Ramillien et al.; 2011, 2012). These KBRR residuals were obtained by correcting the raw GRACE observations from the *a priori* gravitational accelerations of known large-scale mass variations (i.e., atmosphere and oceanic mass variations, polar movements, as well as solid and oceanic tides) during the iterative least-squares orbit adjustment made using the GRGS GINS software (Lemoine et al., 2007; Bruinsma et al., 2010). The effects of non-conservative forces measured by on-board GRACE accelerometers are also removed from the along-track observations, in order to extract the contributions of the remaining not modelled phenomena, thus mainly water mass changes in continental hydrology. Since classical gravimetric inversion does not provide a unique solution and to reduce the spurious effects of the noise in the observations, regularization strategies have been proposed to find numerically stable regional solutions, either based on Singular Value Decomposition (SVD) and L-curve analysis (Ramillien et al., 2011), or by introducing spatial constraints (Ramillien et al., 2012). Time series of successive 10-day regional solutions of water mass have been produced over the whole South America (90°W-30°W; 60°S-20°N) following this regional approach for 2002-2010, and these 2°-by-2° maps revealed realistic amplitudes, for spatial wavelengths lesser than the dimensions of

the region itself by construction (*i.e.*, < 6500 - 8000 km, or equivalently harmonic degrees less than 5-6 for South America). Numerical estimations show us that the predicted regional solutions need to be completed by long wavelength components before being compared with other data sets, when the geographical region is not large enough to contain these long gravity undulations. Over South America, we complemented each regional solution with short and medium wavelengths up to degree 5 from the corresponding GRGS solution (for more details see Ramillien et al., 2012).

2.1.2 ICA-filtered solutions

A post-processing method based on Independent Component Analysis (ICA) was applied to the Level-2 GRACE solutions from different official providers (*i.e.*, UTCSR, JPL and GFZ), after pre-filtering with 400-km-radius Gaussian filters. This approach does not require any *a priori* information, except the assumption of statistical independence between the elementary sources that compose the measured signals (*i.e.*, useful geophysical signals plus noise). Separation consists of finding the independent sources by solving a linear system relating the GRACE solutions provided for a given month, to the unknown independent components. The contributors to the observed gravity field are forced to be uncorrelated numerically by imposing diagonal cross-correlation matrices. For a given month, the ICA-filtered solutions only differ to each other from a scaling factor, so that the GFZ-derived ICA-filtered solutions are only considered. The efficiency of the ICA in separating gravity signals from noise by combining Level-2 GRACE solutions has previously been demonstrated over land (Frappart et al. 2010, 2011b) and ice caps (Bergmann et al., 2012). These monthly ICA solutions are available at: http://grgs.obs-mip.fr. They correspond to what is referred to the first ICA mode (whereas the second and third mode corresponds to the noise) in Frappart et al. (2011b). Time series of ICA-based global maps of

continental water mass changes from combined UTCSR, JPL and GFZ GRACE solutions, computed over the period 08/2002–12/2010, are used in this study. More details about the post-processing can be found in Frappart et al. (2010, 2011b).

2.1.3 GRGS solutions

As for the global Level-2 solutions computed by official providers (CSR, GFZ, and JPL), The Level-2 GRGS-EIGEN-GL04 models are derived from Level-1 GRACE measurements including KBRR, and from LAGEOS-1/2 SLR data for enhancement of lower harmonic degrees (Lemoine et al., 2007; Bruinsma et al., 2010). These gravity fields are expressed in terms of normalized spherical harmonic coefficients of the geopotential (*i.e.*, Stokes coefficients) from degree 2 up to degree 50-60 using an empirical stabilization approach without any smoothing or filtering. This stabilization approach consists in adding empirically-determined degree and order-dependent coefficients to minimize the time variations of the signal measured by GRACE over ocean and desert without significantly affecting the amplitude of the signal over continents. 10-day (Release-2) Total Water Storage (TWS) grids of 1-degree spatial resolution available at http://grgs.obs-mip.fr are used over 2003-2010.

2.2 *In situ* water levels and discharge

Time series of daily water levels from *in situ* gauges located in the largest drainage basins of South America (Amazon, La Plata, Orinoco, Tocantins, São Francisco, Negro) and their tributaries (Fig. 1 and Table 1) and monthly discharges in Obidos (Amazon), Ciudad Bolivar (Orinoco), Tucurui (Tocantins), and Chapeton (La Plata) were used for comparisons to 10-day and monthly anomalies of GRACE-based TWS over 2003-2010. These *in situ* records were downloaded either from the Environmental Research Observatory (ORE) HYBAM website

(http://www.ore-hybam.org/) for the Orinoco basin and some gauges located in the Amazon basin, and from the hydrological information system Hidroweb (http://hidroweb.ana.gov.br/) of the Brazilian water agency (Agência Nacional de Aguas - ANA) for some gauges located in the Amazon and the Tocantins basins, as well as from the Argentinian water agency (Instituto Nacional del Agua –INA) through the online database Base de Datos Hidrológica Integrada (BDHI - http://www.hidricosargentina.gov.ar/) over the period 2002 – 2011. The seasonal amplitude was removed using a 13-month sliding window on each time-serie of daily *in situ* water levels and monthly discharge.

2.3 Maps of water resources

2.3.1 Floodplains, wetlands and lakes database

The Global Land and Wetlands Database (GLWD) based on the combination of different available cartographic sources is a comprehensive database of global lakes with an area greater than 1 km² and provides a good representation of the maximum global wetland extent (Lehner and Döll, 2004). We used the GLWD-3 product with a spatial resolution of 30' to locate the surface waters (*i.e.*, large-scale wetland distributions and important wetland complexes) over South America.

2.3.2 Groundwater resources map

The Worldwide Hydrological Mapping and Assessment Programme (WHYMAP) made available a 1:25,000,000 map of groundwater resources through the website of the German Federal Institute for Geosciences and Natural Resources (Bundesanstalt für Geowissenschaften un Rohstoffe - BGR): http://www.whymap.org. This map presents the geographical extent of the aquifers and their environmental charcateristics: large and rather uniform groundwater basins, complex hydrogeological structures, and limited groundwater resources in local and shallow

aquifers (Richts et al., 2011). The groundwater recharge information originates from WGHM model outputs (Döll and Fiedler, 2008).

2.4 Time-series of TWS expressed in terms of equivalent sea level at basin-scale

For a given month *t*, regional average of TWS expressed in terms of mm of equivalent-water height ($\Delta h_{TWS}(t)$) over a given river basin of area *S* is computed from the TWS anomaly grid ($\Delta h(\lambda_j,\varphi_j,t)$) at time *t* of the pixel of longitude and latitude (λ_j,φ_j) with $j=1, 2, \ldots$ inside *S*, and the elementary surface $R_e^2 \Delta\lambda \Delta\varphi \cos\varphi_j$ (Ramillien et al., 2005; Frappart et al., 2011a):

$$\Delta h_{TWS}(t) = \frac{R_e^2}{S} \sum_{j \in S} \Delta h\left(\lambda_j, \varphi_j, t\right) \cos\left(\varphi_j\right) \Delta\lambda \Delta\varphi \qquad (1)$$

where R_e is the mean radius of the Earth (6378 km) and $\Delta\lambda$ and $\Delta\varphi$ are the grid steps in longitude and latitude respectively (generally $\Delta\lambda = \Delta\varphi$).

The time-series of TWS expressed in EWH for the four largest South American drainage basins are then converted into Equivalent Sea Level (ESL) ($\Delta h_{TWS\_ESL}(t)$) (Ramillien et al., 2008b):

$$\Delta h_{TWS\_ESL}(t) = \frac{\rho_{SW} S_{basin}}{\rho_{ocean} S_{ocean}} \Delta h_{TWS}(t) \qquad (2)$$

where ρ_{SW} and ρ_{ocean} are the densities of soil water and ocean (with the respective values of 1,000 and 1,030 kg.m^{-3}), and S_{basin} and S_{ocean} the surfaces of the considered basin and the global ocean (S_{ocean} = 360 millions of km²) respectively.

3. Results

3.1 PCA modes of TWS at interannual time-scale

A Principal Components Analysis (PCA) was applied to the series of GRACE-based TWS from Regional, ICA, and GRGS solutions over South America (-90° - -30°; -60° - 20°) for the period

2003-2010, after removal of the dominant seasonal amplitude using a 13-month sliding window. The sum of the explained variances (σ^2) of the four first PCA modes represents 0.87 for the regional, 0.82 for the ICA-GFZ-400km (0.83 for both ICA-CSR-400km and ICA-JPL-400km), and 0.92 for the GRGS solutions (Table 2). The explained variance by a mode corresponds to the variance in the dataset explained by a PC, the sum of the variances or total variance equals 100%. Most of the seasonally corrected signal present in the GRACE-derived land water solutions is mostly concentrated in these four modes that will be analyzed in detail in the following.

The resulting 4 first modes are respectively presented in Fig. 2, 4, 6, and 8 for the spatial components and in Fig. 3, 5, 7, 9 for the temporal components. Spatial components of the 4 first modes exhibit similar patterns for the different GRACE solutions. Correlations between pairs of GRACE solutions for each spatial mode can be found in Table 3. They are generally higher between regional and ICA solutions than between regional and GRGS solutions (*i.e.*, $R_{(regional;\ ICA)} - R_{(regional;\ GRGS)} > 0.23$), except for the fourth mode. The major difference between the regional and the global solutions is the complete absence in the regional solutions of spurious meridional undulations materialized as north-south stripes, and unfortunately polluting the spatial patterns of the global ones. These north-south stripes appear as one the major features in the 1st spatial mode of the GRGS solutions (Fig. 2c), and can also be identified in the 2nd spatial mode of the GRGS (Fig. 4c), as well as in the 1st and 4th spatial modes of the ICA solutions (Fig. 2b and Fig. 8b respectively) but with a lower intensity. The presence of these stripes account for the lower agreement between the 1st mode of GRGS and regional (but also ICA) solutions (Table 3). Besides, for the 2nd and 3rd modes, this lower agreement results from the different geographical locations of the extrema.

236 The large negative pattern located above the Equator in the 2nd mode of the regional and ICA
237 solutions (Fig. 4a and b respectively) is centered on the Equator in the 2nd mode of the GRGS
238 solutions (Fig. 4c). The two maxima centered around -70° of longitude and -5° of latitude, and -
239 70° of longitude and -5° of latitude (Fig. 4a and b respectively), in the 2nd mode of the regional
240 and ICA solutions, are absent from the 2nd mode of the GRGS solutions (Fig. 4c). Accordingly,
241 the maximum and minimum located on the right and left banks of the Amazon have a different
242 shape in the 3rd mode of the regional and ICA solutions (Fig. 6a and b respectively), and in the 3rd
243 mode of the GRGS solutions (Fig. 6c). This different behavior of the GRGS products compared
244 with other regional and global solutions has already been reported by Klees et al. (2008) over
245 different large continental areas and river basins, and lately by Awange et al. (2011) over
246 Australia. It was attributed to leakage effect (Klees et al., 2008) caused by the low cut-off degree
247 applied to GRGS solutions (*i.e.*, n=50 or spatial resolution of 400 km) compared to the one
248 applied to other global solutions (*i.e.*, n=60 for CSR and n=120 for GFZ and JPL, or spatial
249 resolutions of 333 km and 167 km respectively), and moreover to the north-south striping largely
250 affecting these global solutions (Awange et al., 2011). For the 4th mode, the lower agreement
251 between regional and ICA solutions can be attributed to the smoothness of these solutions that are
252 twice filtered using a Gaussian filter of 400 km of radius before being separated by ICA.

253 Temporal components of the four 1st modes of the PCA of the GRACE solutions also present
254 quite similar profiles. Cross-correlations between pairs of GRACE solutions for each temporal
255 mode were also computed for time-lag (Δt) varying between ± 6 months. Results are presented in
256 Table 4 for Δt=0 and Δt maximizing the cross-correlation into the one-year window. Similarly to
257 what was earlier revealed for the spatial components, greater correlations are found between the
258 regional and the ICA solutions than between the regional and the GRGS solutions for smaller

time-delays, except for the 4th mode (Table 4). Similar large time-shifts between GRGS and other types of GRACE solutions were already observed over Australia and attributed to the large impact of degrading north-south striping on the restitution of the hydrological signals, especially at interannual time-scales (Awange et al., 2011).

3.2 Relationships between main TWS modes and hydrological features of South America

3.2.1 First mode of variability

South America is covered by large drainage basins where surface waters represent a large part of the TWS measured by GRACE (Frappart et al., 2008; 2011c; 2012; Han et al., 2009; Kim et al., 2009). So, the spatial and temporal components of the PCA of the GRACE-based TWS are respectively compared to the spatial distribution of lakes and reservoirs, rivers and associated floodplains, and wetlands from GLWD (Lehner and Döll, 2004), and the interannual variations of water levels at the mouth of the South America's major rivers and tributaries (see the location of the selected in situ gauges in Fig. 1). We deliberately limited our analysis to the *in situ* gauges at located at (or close to) the mouth of a (sub-)basin, to be representative of a sufficiently large drainage area, to remain compatible with the spatial resolution of the GRACE-based hydrological products (*i.e.*, 300-400 km).

The spatial component of the PCA first mode is presented in Fig. 2a-c for respectively regional (σ^2=0.43), ICA-CSR-400 km (σ^2=0.44), noted ICA in the followings, and GRGS (σ^2=0.6) land water solutions. In spite of the coarse spatial resolution of the GRACE data, it agrees well with the distribution of surface water from GLWD (Fig. 2d). The strongest amplitudes of the first mode are located in the Altiplano region, area of inland in the Central Andes encompassing Titicaca and Poopó lakes, along the Solimões-Amazon corridor (including the south of the Amazonian and the Negro basins), in the delta of La Plata, upstream the mouth of the Tocantins,

283 and in the region covered with Pindare and Parnacaiba basins (Fig. 2d). Some secondary extrema
284 are also seen at the mouth of the Orinoco basin, the region of the sources of the Parana (La Plata)
285 and São Francisco rivers, and in the Deseado basin in Patagonia and over Patagonia Icefield (Fig.
286 2d). These hydrological structures are better concentrated on the regional (Fig. 2a) than on the
287 global spherical harmonics solutions (Fig. 2b and c). One of the main advantages in considering
288 regional solutions is to concentrate the starting GRACE information in a chosen portion of the
289 terrestrial surface (*i.e.*, better spatial localization), instead of dealing with global spectral
290 coefficients (*i.e.*, best frequency localization) (see Freeden and Schreiner, 2008). In the latter
291 case, by construction, the satellite signals are diluated over all the terrestrial sphere, consequently
292 any sharp surface detail should be reconstructed by a quasi-infinite sum of spherical harmonic
293 coefficients, which remains impossible in practice as GRGS and ICA solutions are limited up to
294 degree 50-60. The associated temporal component for each GRACE solutions is presented in Fig.
295 3a. The three time-series appear very similar, however the GRGS one being smoother. The
296 regional and the ICA solutions exhibit larger negative peaks in 2005 and 2010, and positive in
297 2009, corresponding to the extreme droughts and flood which strongly affected the Amazon basin
298 (Chen et al., 2009; 2010a; Marengo et al., 2011; Tomasella et al., 2011; Frappart et al., 2012; in
299 press), and to the 2009 drought that affected La Plata Basin (Chen et al., 2010b; Pereira and
300 Pacino, 2012), than the GRGS solutions. Regional and ICA solutions are almost in phase except
301 for the 2009 extreme flood when the ICA peak is located in the beginning of the year whereas it
302 occurs later (April-May) in the regional solutions, close to the flood peak in the Amazon basin.

303 Comparisons to *in situ* gauges highly (anti)correlated to mode 1 are presented in Fig. 3b and
304 Table 5. Please note that anti-correlations come from the arbitrary sign given to both the spatial

and temporal components. In all cases, the anti-correlation corresponds to region where the spatial mode has a negative sign.

Mode 1 represents the larger part of the variability observed over South America in the GRACE solutions. It is logically correlated to the largest number of *in situ* stations used in this study (9 among 18 or 50% with $|R|>0.65$ for the regional solutions), and to *in situ* stations (Fig. 1) located in a neighborhood of an extremum or a secondary extremum in the spatial component. Correlations are generally higher for the regional solutions, than for the ICA and GRGS solutions, even if the values are quite high for all type of solutions. High correlation (>0.8) is observed in Obidos located at ~1500 km upstream to the mouth of the Amazon, for all type of solutions with different time-delays between the GRACE solutions and the *in situ* measurements: -20/30/-120 days between regional/ICA/GRGS solutions and water levels in Obidos respectively (Table 5). The zero time-lag corresponds to the region of maximum of signal located between Jatuarana and Obidos (see Fig. 1), in the centre of the downstream Amazon along its mainstem. The opposition of phase between the hydrological signals in the Orinoco and the Amazon basins clearly appears in the time lags for Obidos and Ciudad Bolivar in the regional and ICA solutions. A higher delay is observed upstream in the Madeira tributary at Fazenda Vista Alegre, a much higher one in Manaus, due to the control of the Negro river flow by the Solimões or backwater effect (Meade et al., 1991). On the contrary, negative time-lag is found for the Xingu river, in the regional, and mostly, in the ICA solutions (except for Itaituba and Manaus).

This confirms that the Regional solutions are more accurate as they are both spatially and temporally better localized than the global solutions. A large decrease of mass can be identified in the Patagonian Icefield between 2003 and 2009, as a positive trend in the temporal component

is multiplied by negative values in the spatial component. This confirms what was already observed by Chen et al. (2007) using GRACE data.

3.2.2 Second mode of variability

The spatial components of the second mode of PCA are presented in Fig. 4a-c for Regional (σ^2=0.2), ICA (σ^2=0.15), and GRGS (σ^2=0.14) land water solutions, respectively. The extrema present in the Regional (Fig. 4a) and ICA (Fig. 4b) are centred on the Orinoco and the Negro basins (*i.e.*, negative patterns in the northern part of South America), the southern bank of the Solimões, the region covered with both Pindare and Parnacaiba basins, and the downstream part and the delta of La Plata basin (positive patterns in the western, eastern, and south eastern parts of the continent respectively). These structures are in good agreement with the distribution of surface water from GLWD (Fig. 4d). The spatial patterns of the 2nd mode of PCA for the GRGS is quite different, as a large negative pattern appears on the central corridor of the Amazon, at the junction between the Solimões, Negro and Madeira rivers, and no positive pattern over the southern bank of the Solimões, and neither in the region covered with Pindare and Parnacaiba basins.

Four *in situ* stations (~20%) were found to have high correlations with the 2nd mode temporal mode of the PCA of the GRACE-derived TWS (Table 5). Three of them are located in the Amazon basin: one in the Branco basin, sub-basin of the Negro basin, northern Amazon where high correlations are obtained ($|R|>0.8$), especially for the regional and the ICA solutions, and two in the Solimões basin, at its entrance (Tabatinga) and its mouth (Manacapuru). For these two latter stations, high correlations are found between *in situ* water levels and GRACE-based TWS from regional and ICA solutions, but not from GRGS ($R<0.5$) (Table 5). The last one is located in La Plata basin and better agreement is found between these water level records and GRGS-

derived solutions than regional-derived and ICA-derived solutions. This appears clearly on Fig. 5 presenting the temporal component of the 2nd PCA mode for each set of GRACE solutions (Fig. 5a) and the time-series of *in situ* water levels for these 4 four stations (Fig. 5b). A time lag of nine months clearly separate the maxima of regional and ICA solutions (*i.e.*, northern hemisphere summer 2009) to the maximum of GRGS solutions (*i.e.*, northern hemisphere winter 2010). They respectively correspond to the extreme flood that affected the Amazon basin in 2009 (Marengo et al., 2011) and to a flooding event occurring in La Plata basin from December 2009 to April 2010 (Salvia et al., 2011).

3.2.3 Third mode of variability

The spatial component of the third PCA mode is presented in Fig. 6a-c for regional (σ^2=0.13), ICA (σ^2=0.14), and GRGS (σ^2=0.1) land water solutions respectively (Table 2). As for mode 2, a better agreement is found between regional and ICA solutions than between regional and GRGS solutions, with correlation coefficients equal to 0.69 and 0.46 respectively (Table 3). The maxima in the regional (Fig. 6a) and ICA (Fig. 6b) are located in the southern bank of the Solimões and the central corridor of the Amazon river up to its junction with the Tapajos river, and the upstream part of the Tocantins basin. Once again, this structure is in good agreement with the distribution of surface water from GLWD (Fig. 6d). Some secondary extrema can also be observed in the Negro basin in Argentina, over the Patagonia Icefield and Deseado basin in Patagonia in the south. In the north, extrema are centred over the Essequibo (Guyana), Suriname (Suriname), Oyapok and Maroni (French Guiana) basins (negative). GRGS solutions show that the extrema are located around the central corridor of the Amazon river: negative in the north (northern tributaries and Orinoco). Positive extrema appear in the south and over the Tocantins, Pindare, and Parnacaiba basins for the GRGS solutions.

Its temporal component was found to be correlated ($|R| > 0.7$) to the time-variations of three in situ stations (~15%) located in the Tocantins (Tucurui) and the eastern and southern parts of La Plata (Chapeton and Pepiri Mini), for the regional and ICA solutions. However, the temporal mode for the GRGS solutions is not correlated to *in situ* records (Table 5).

3.2.4 Fourth mode of variability

The spatial component of the fourth PCA mode is presented in Fig. 8a-c for regional (σ^2=0.11), ICA (σ^2=0.1), and GRGS (σ^2=0.08) land water solutions respectively (Table 2). Correlation is much higher between regional and GRGS solutions (R=0.86) than between regional and ICA solutions (R=0.46) (Table 3). North-south stripes clearly appear for the ICA solutions (Fig. 8b). Patterns of TWS seem to be related to the spatial distribution of groundwater recharge from WHYMAP (Fig. 8d). Positive and negative extrema of TWS are located over regions where recharge is maximum: the central corridor of the Amazon river, the downstream part of the Tocantins, the Pindare and the Parnacaiba, and the eastern part of La Plata basin (Fig. 8d). They correspond to the locations of the largest aquifers of South America: Amazonas and Maranhão basins, Guarani Aquifer System respectively (Margat, 2007), and to a region of high to very high recharge according to WHYMAP, located between the two latter basins, which makes part of the groundwater footprint (*i.e.*, the area required to sustain groundwater use and groundwater-dependent ecosystem services of a region of interest, such as an aquifer, watershed or community) of the Maranhão according to Gleeson et al. (2012) (see Fig. 1 of this paper). The temporal component of the fourth mode is highly correlated to the time-series of water levels of two *in situ* stations (~10%) located in the São Francisco and the Negro (in Argentina) basins.

3.3 Contribution to the major South American drainage basins to sea level

3.3.1 Time series of equivalent sea level in large drainage basins

By dividing the water volume variations by the total ocean surface (~360 millions of km^2), the Equivalent Sea Level (ESL) time series are simply obtained (Fig. 10). They correspond to the water mass contributions of these drainage basins to the actual measured sea level. The ESL time series of regional, GRGS and ICA-400 km solutions remain very close to each other. However, GRGS-based solutions present slightly greater amplitudes when they are averaged over the South American basins. In general, the ESL time series are dominated by a strong seasonal cycle, as previous shown by Ramillien et al. (2008b) while using 3-year GRACE data, that reaches +/-2 mm for the Amazon river basin. This latter river basin appears as the largest contributor of water mass to the oceans at annual time scale, while the three others have amplitudes of +/-0.5 mm ESL. Besides, these series exhibit clear multi-year variations and modulations of the dominant seasonal cycle: in the case of the Amazon, the maxima are important (up to 4 mm ESL) in 2006, 2008 and 2009 only, whereas the curve for La Plata basin contains short wavelengths with maxima of seasonal cycle in 2003, 2007 and 2010. As both time-series of 10-day solutions (*i.e.*, regional and GRGS) exhibit important "high-frequency" variations, their origin seems to be related to sub-monthly hydrological events. Analysis of daily water levels over 37 years (1961-1997) at Corrientes, the closest station to the mouth of La Plata basin, shows larger standard deviations for a lower annual cycle than a similar analysis performed in Obidos (over 27 years), the closest station to the mouth of La Plata basin (Clarke et al., 2000). This suggests important short-term hydrological variations in the surface reservoir that can account for the rapid variations observed in Fig. 10d.

3.3.2 Interannual variations of TWS and discharges in large drainage basins

420 The contribution to sea level variations at interannual time-scale of the largest drainage basins of
421 South America (*i.e.*, Amazon, Orinoco, and Tocantins) is presented on Fig. 11. If the 12-month
422 cycle is removed by applying a 13-month average sliding window on each ESL time-series, it is
423 clear the inter-annual residuals will not be explained by a simple linear trend for the considered
424 2003-2010 period (Fig. 11). The signatures of the extreme and sudden climatic events that
425 recently affected the Amazon basin as the droughts of 2005 and 2010 and the flood of 2009 (Fig.
426 11a), and La Plata such as the drought of 2009 and the flood of 2010 (Fig. 11d) can be clearly
427 identified. This is in contradiction with the self-made idea that continents would provide (or
428 retain) water mass to the oceans continuously, by suggesting multi-year variations do not permit
429 to establish a definitive water mass balance. Moreover, errors in the determination of the long-
430 term mass balance remain comparable to the fitted linear trend values themselves (~0.03 mm/yr),
431 according to Ramillien et al. (2008b). In the case of spherical harmonics representation (*i.e.*,
432 GRGS and ICA solutions), most of uncertainty (up to 0.05 mm ESL) is due to spectral leakage
433 (i.e., pollution of signals from other parts of the globe) because of truncation at degree 50-60
434 (Frappart et al., 2011b). This motivates us to compare the inter-annual variations to independent
435 datasets such as discharge change measurements versus time, to confirm the quality of our water
436 mass estimates computed from the different GRACE datasets. The interannual variations of TWS
437 are compared to the interannual variations of river discharges for these large drainage basins of
438 South America. They exhibit similar patterns as already observed in the Amazon basin and its
439 sub-basins using the ICA solutions (Frappart et al., 2012; in press). High correlations ($R \geq 0.9$)
440 were found in the Amazon basin with one month of delay between TWS and discharge (Table 6).
441 This delay can be accounted for the presence of extensive floodplains along the central corridor
442 of the Amazon-Solimões, and over Negro (northern tributary of the Amazon) and Mamoré
443 basins, that cover more than 300,000 km² of the surface of the basin (Diegues, 1994; Junk, 1997).

The presence of floodplains delays the transit of surface water. As a consequence, TWS is dominated by surface water causing a time-shift between TWS and discharge. On the contrary, for basins less densely covered with floodplains as the Orinoco and La Plata, correlation in time between TWS and discharge remains high (R~0.7 except for the ICA solutions with R~0.6 and R>0.75 except for the ICA solutions with R~0.6 respectively), however the time shift is negative: maximum of discharge occurs one or two months before the maximum of TWS (Table 6). In the Tocantins basin, correlation between TWS and discharge is much lower (R<0.6) most likely because the interannual variations of TWS are more influenced by the groundwater storage, as the region is characterized by the presence of a large aquifer system (Maranhão basin).

4. Conclusion

2-by-2 degree regional water mass solutions over South America were compared to GRACE-based global products (GRGS and ICA-400) for the period 2003-2010, and it is shown that they offer a better geographical location of hydrological structures by construction than global solutions. As a consequence, the higher power spectral density present in the regional solution at at smaller spatial scales can be attributed to a better determination of these wavelengths in the regional solutions. Besides, the global GRGS solutions suffer from the presence of residuals North-South striping from aliasing, this effect masks the hydrological structures, and consequently degrades the water mass balance estimates. Principal Component Decomposition of all the GRACE datasets permitted us to unravel modes of variability from observed signals observed by GRACE, and then identify geographical locations of inter-annual water mass variations of individual groundwater unit over the continent, and correlate them to climatology. Robust validation of these GRACE datasets consists of comparing them to time variations of *in situ* water level and discharge measurements. Correlations between GRACE solutions and river

level records are significant for the four first PCA modes suggesting these modes represent water mass changes at the surface of the Earth. In particular, signature of the melt of the Patagonian IceField in the gravity field is found in temporal modes 1 and 3 while its location is well identified in the corresponding spatial modes. Temporal mode number 4 seems to be mostly related to slower groundwater variations, as the corresponding spatial mode clearly coincides with the geographical limits of groundwater unit. High correlations are also found between TWS and river discharges at interannual time-scale in the Amazon and Orinoco basins where TWS is dominated by the surface reservoir due to the presence of extensive floodplains, whereas low correlation is found for the Tocantins, likely because the measured gravity signal is dominated by groundwater changes in this basin. Our study, based on the use of PCA, demonstrated the ability of GRACE satellite gravimetry to distinguish efficiently real hydrological signals in different reservoirs (surface waters, groundwater, glaciers) especially through such a regional approach.

5. Acknowledgements

The authors would like to thank Dr. Wilhelm Struckmeier and Dipl.-Geogr. Andrea Richts from BGR for letting us use the WHYMAP map of groundwater resources in their paper.

6. References

Alsdorf, D. E., & Lettenmaier, D.P. (2003). Tracking fresh water from space. *Science, 301,* 1492-1494.

Andersen, O. B., Seneviratne, S.I., Hinderer, J. & Viterbo, P. (2005). GRACE-derived terrestrial water storage depletion associated with the 2003 European heat wave. *Geophysical Research Letters, 32(18),* L18405.

Awange, J.L., Fleming, K.M., Kuhn, M., Featherstone, W.E., Heck, B., & Anjasmara, I. (2011). On the suitability of the 4°x4° GRACE mascon solutions for remote sensing Australian hydrology. *Remote Sensing of Environment, 115(3),* 864-875.

Bergmann, I., Ramillien, G., & Frappart, F. (2012). Climate-driven interannual variations of the mass balance of Greenland. *Global and Planetary Change, 82-83*, 1-11, doi: 10.1016/j.gloplacha.2011.

Bruinsma, S., Lemoine, J-M., Biancale, R., & Valès, N. (2010). CNES/GRGS 10-day gravity models (release 2) and their evaluation. *Advances in Space Research, 45(4)*, 587–601, doi:10.1016/j.asr.2009.10.012.

Chen, J.L., Wilson, C.R., Tapley, B.D., Blankenship, D.D., & Ivins, E.R. (2007). Patagonia Icefield melting observed by Gravity Recovery and Climate Experiment (GRACE). *Geophysical Research Letters, 34(22)*, L22501.

Chen, J.L., Wilson, C.R., Tapley, B.D., Yang, Z.L. & Niu G.Y. (2009). 2005 drought event in the Amazon River basin as measured by GRACE and estimated by climate models, *Journal of Geophysical Research, 114*, B05404, doi:10.1029/2008JB006056.

Chen, J.L., Wilson, C.R., & Tapley, B.D. (2010a). The 2009 exceptional Amazon flood and interannual terrestrial water storage change observed by GRACE. *Water Resources Research, 46(12)*, W12526. doi: 10.1029/2010WR009383.

Chen, J.L., Wilson, C.R., Tapley, B.D., Longuevergne, L., Yang, Z.L., & Scanlon, B.R. (2010b). Recent La Plata basin drought conditions observed by satellite gravimetry. *Journal of Geophysical Research, 115*, D22108, doi: 10.1029/2010JD014689.

Clarke, R.T., Mendiondo, E.M., & Brusa L.C. (2000). Uncertainties in mean discharges from two large South American rivers due to rating curve variability. *Hydrological Sciences Journal-Journal Des Sciences Hydrologiques, 45(2)*, 221–236.

Diegues A.C.S. (ed.) (1994). *An Inventory of Brazilian Wetlands*, International Union for Conservation of Nature, Gland, Switzerland, 224 pp.

Döll, P., & Fiedler, K. (2008). Global-scale modeling of groundwater recharge. *Hydrology and Earth System Sciences, 12*, 863–885, doi:10.5194/hess-12-863-2008.

Eicker, A. (2008). *Gravity Field Refinement by Radial Basis Functions from In-situ Satellite Data*. Dissertation Univ. Bonn D 98, pp. 137, Univ. Bonn, Bonn, Germany.

Frappart, F., Papa, F., Famiglietti, J.S., Prigent, C., Rossow, W.B., & Seyler, F. (2008). Interannual variations of river water storage from a multiple satellite approach: a case study for the Rio Negro River basin. *Journal of Geophysical Research, 113(D21)*, D21104, doi: 10.1029/2007JD009438.

Frappart, F., Ramillien, G., Maisongrande, P., & Bonnet, M-P. (2010). Denoising satellite gravity signals by independent component analysis. *IEEE Geoscience and Remote Sensing Letters, 7(3)*, 421–425, doi:10.1109/LGRS.2009.2037837.

542 Frappart, F., Ramillien, G., & Famiglietti, J.S. (2011a). Water balance of the Arctic drainage
543 system using GRACE gravimetry products. *International Journal of Remote Sensing, 32(2)*, 431-
544 453, doi: 10.1080/01431160903474954.
545
546 Frappart, F., Ramillien, G., Leblanc, M., Tweed, S.O., Bonnet, M-P., & Maisongrande, P.
547 (2011b). An independent component analysis approach for filtering continental hydrology in the
548 GRACE gravity data. *Remote Sensing of Environment, 115(1)*, 187-204,
549 doi:10.1016/j.rse.2010.08.017.
550
551 Frappart, F., Papa, F., Güntner, A., Werth, S., Santos da Silva, J., Seyler, F., Prigent, C., Rossow,
552 W.B., Calmant, S., & Bonnet, M-P. (2011c). Satellite-based estimates of groundwater storage
553 variations in large drainage basins with extensive floodplains. *Remote Sensing of Environment*,
554 *115(6)*, 1588-1594, doi: 10.1016/j.rse.2011.02.003.
555
556 Frappart, F., Papa, F., Santos da Silva, J., Ramillien, G., Prigent, C., Seyler, F., & Calmant, S.
557 (2012). Surface freshwater storage in the Amazon basin during the 2005 exceptional drought.
558 *Environmental Research Letters*, *7(4)*, 044010, doi:10.1088/1748-9326/7/044010.

559 Frappart, F., Ramillien, G., & Ronchail, J., (in press). Changes in terrestrial water storage vs.
560 rainfall and discharges in the Amazon basin. *International Journal of Climatology*, in press.
561
562 Freeden, W., & Schreiner, M. (2008). *Spherical Functions of Mathematical Geosciences: A*
563 *Scalar, Vectorial, and Tensorial Setup*, Springer, Heidelberg, 602 pp.
564
565 Gleeson, T., Wada, Y., Bierkens, M.F.P., & van Beek, L.P.H. (2012). Water balance of global
566 aquifers revealed by groundwater footprint. *Nature, 488*, 197-200, doi: 10.1038/nature11295.
567
568 Han, S-C., Kim, H., Yeo, I.Y., Yeh, P., Oki, T., Seo, K.W., Alsdorf, D., & Luthcke, S.B. (2009).
569 Dynamics of surface water storage in the Amazon inferred from measurements of inter-satellite
570 distance change. *Geophysical Research Letters, 36*, L09403, doi: 10.1029/2009GL037910.

571 Junk, W.J. (1997). General aspects of floodplain ecology with special reference to Amazonian
572 floodplains, in *The central Amazon floodplain: Ecology of a pulsing system* (Junk, W.J., Piedade,
573 M.T.F., Wittmann, F., Schöngart, J., & Parolin, P., eds), 3-20, Springer-Verlag, Berin &
574 Heidelberg, Germany.
575
576 Kim, H., Yeh, P.J.F., Oki, T., & Kanae, S. (2009). Role of rivers in the seasonal variations of
577 terrestrial water storage over global basins. *Geophysycal Research Letters, 36*, L17402, doi:
578 10.1029/2009GL039006.
579
580 Klees, R., Liu, X., Wittwer, T., Gunter, B.C., Revtova, E.A., Tenzer, R., Ditmar, P., Winsemius,
581 H.C., & Savenije, H.H.G. (2008). A comparison of global and regional GRACE models for land
582 hydrology. *Surveys in Geophysics, 29(4-5)*, 335−359.
583
584 Lehner, B., & Döll, P. (2004). Development and validation of a global database of lakes,
585 reservoirs and wetlands. *Journal of Hydrology, 296(1-4)*, 1-22.

Leblanc, M. J., Tregoning, P., Ramillien, G., Tweed, S.O., & Fakes, A. (2009). Basin‐scale, integrated observations of the early 21st century multiyear drought in southeast Australia. *Water Resources Research*, *45*, W04408, doi:10.1029/2008WR007333.

Lemoine, J-M., Bruinsma, S., Loyer, S., Biancale, R., Marty, J-C., Pérosanz, F., & Balmino, G. (2007). Temporal gravity field models inferred from GRACE data. *Advances in Space Research, 39(10)*, 1620–1629.

Marengo, J.A., Tomasella, J., Soares, W., Alves, L.M., & Nobre, C. (2011). Extreme climatic events in the Amazon basin: climatological and hydrological context of recent floods. *Theoretical and Applied Climatology, 107(1-2)*, 73–85, doi: 10.1007/s00704-011-0465-1.

Margat, J. (2007). Great aquifer systems of the world. *In Aquifer Systems Management: Darcy's Legacy in a World of Impending Water*. Chery L. and de Marsily G. (Eds.), 105-116, Taylor and Francis, Oxford, England.

Meade, R.H., Rayol, J.M., Conceição, S.C., & Navidade, J. R.G. (1991). Backwater effects in the Amazon basin of Brazil. *Environmental Geology and Water Science*, *18*, 105–14.

Pereira, A., Pacino, M.C. (2012). Annual and seasonal water storage changes detected from GRACE data in the La Plata Basin. *Physics of the Earth and Planetary Interiors*, *212–213*, 88-99, doi: 10.1016/j.pepi.2012.09.005.

Ramillien, G., Frappart, F., Cazenave, A., & Güntner, A. (2005). Time variations of land water storage from the inversion of 2-years of GRACE geoids. *Earth and Planetary Science Letters, 235(1-2)*, 283-301, doi:10.1016/j.epsl.2005.04.005.

Ramillien, G., Frappart, F., Güntner, A., Ngo-Duc, T., Cazenave, A. & Laval, K. (2006). Time variations of the regional evapotranspiration rate from Gravimetry Recovery And Climate Experiment (GRACE) satellite gravimetry. *Water Resources Research, 42*, W10403, doi:10.1029/2005WR004331.

Ramillien, G., Famiglietti, J.S., & Wahr, J. (2008a). Detection of continental hydrology and glaciology signals from GRACE: a review. *Surveys in Geophysics*, *29*, 361-374, doi: 10.1007/s10712-008-9048-9.

Ramillien, G., Bouhours, S., Lombard, A., Cazenave, A., Flechtner, F., & Schmidt, R. (2008b). Land water storage contribution to sea level from GRACE geoid data over 2003-2006. *Global and Planetary Change, 60(3-4)*, 381-392, doi:10.1016/j.gloplacha.2007.04.002.

Ramillien, G., Biancale, R., Gratton, S., Vasseur, X., & Bourgogne, S. (2011). GRACE-derived surface mass anomalies by energy integral approach. Application to continental hydrology. *Journal of Geodesy, 85(6)*, 313–328, doi:10.1007/s00190-010-0438-7.

630 Ramillien, G., Seoane, L., Frappart, F., Biancale, R., Gratton, S., Vasseur, X., & Bourgogne, S.
631 (2012). Constrained regional recovery of continental water mass time-variations from GRACE-
632 based geopotential anomalies over South America. *Surveys in Geophysics, 33*, 887-905, doi:
633 10.1007/s10712-012-9177-z.
634
635 Richts, A., Struckmeier, W.F., & Zaepke, M. (2011). WHYMAP and the groundwater resources
636 map of the world 1:25,000,000, *In Sustaining Groundwater Resources: A Critical Element in the*
637 *Global Water Crisis*, Jones J.A.A. (Ed.), 159-173, Springer, Netherlands, doi: 10.1007/978-90-
638 3426-7_10.
639
640 Rodell, M., Famiglietti, J.S., Chen, J., Seneviratne, S.I., Viterbo, P., Holl S. & Wilson C.R.
641 (2004). Basin scale estimates of evapotranspiration using GRACE and other observations.
642 *Geophysycal Research Letters, 31(20)*, L20504.

643 Rodell, M., Chen, J., Kato, H., Famiglietti, J.S., Nigro, J. & Wilson, C. (2007). Estimating
644 groundwater storage changes in the Mississippi River basin (USA) using GRACE. *Hydrogeology*
645 *Journal, 15*(1), 159-166.

646 Rowlands D.D., Luthcke, S.B., Klosko, S.M., Lemoine, F.G.R., Chinn, D.S., McCarthy, J.J.,
647 Cox, C.M., & Anderson, O.B. (2005). Resolving mass flux at high spatial and temporal
648 resolution using GRACE intersatellite measurements. *Geophysical Research Letters, 32*, L04310,
649 doi:10.1029/2004GL021908.

650 Rowlands, D.D., Luthcke, S.B., McCarthy, J.J., Klosko, S.M., Chinn, D.S., Lemoine, F.G., Boy,
651 J-P., & Sabaka, T.J. (2010). Global mass flux solutions from GRACE: A comparison of
652 parameter estimation strategies - Mass concentrations versus Stokes coefficients. *Journal of*
653 *Geophysical Research, 115*, B01403, doi:10.1029/2009JB006546.

654 Salvia, M., Grings, F., Ferrazzoli, P., Barraza, V., Douna, V., Perna, P., Bruscantini, C. &
655 Karszenbaum, H. (2011). Estimating flooded area and mean water level using active and passive
656 microwaves: the example of Parana River Delta floodplain. *Hydrology and Earth System*
657 *Sciences, 15*, 2679-2692, doi: 10.5194/hess-15-2679-2011.

658 Schmidt, R., Flechtner, F., Meyer, U., Neumayer, K.-H., Dahle, Ch., Koenig, R., & Kusche, J.
659 (2008). Hydrological Signals Observed by the GRACE Satellites. *Surveys in*
660 *Geophysics, 29*, 319–334, doi: 10.1007/s10712-008-9033-3.

661 Seitz, F., Schmidt, M. & Shum, C.K. (2008). Signals of extreme weather conditions in Central
662 Europe in GRACE 4-D hydrological mass variations, *Earth and Planetary Science Letters,*
663 *268(1-2)*, 165-170.

664 Strassberg, G., Scanlon, B. R., & Rodell, M. (2007). Comparison of seasonal terrestrial water
665 storage variations from GRACE with groundwater-level measurements from the High Plains
666 Aquifer (USA). *Geophysical Research Letters, 34*, L14402, doi:10.1029/2007GL030139.

667 Syed, T.H., Famiglietti, J.S., & Chambers, D. (2009). GRACE-based estimates of terrestrial
668 freshwater discharge from basin to continental scales. *Journal of Hydrometeorology, 10(1)*, doi:
669 10.1175/2008JHM993.1.

670 Tapley, B.D., Bettadpur, S., Ries, J.C., Thompson, P.F., & Watkins M. (2004). GRACE
671 measurements of mass variability in the Earth system. *Science, 305*, 503-505.

672 Tomasella, J., Borma, L.S., Marengo, J.A., Rodriguez, D.A., Cuartas, L.A., Nobre, C.A., Prado,
673 M.C.R. (2011). The droughts of 1996-1997 and 2004-2005 in Amazonia: hydrological response
674 in the river main-stem. *Hydrological Processes, 25*, 1228-1242, doi: 10.1002/hyp.7889.

675

List of Tables

List of Figures

Figure 1 : Major drainage basins of South America: Orinoco (light green), Amazon (dark blue), Tocantins (red), São Francisco (dark green), La Plata (grey), Negro (orange). *In situ* gauge stations are represented with red circles (HYBAM), black squares (ANA), and green triangles (INA).

Figure 2 : Spatial component of the 1st PCA mode of TWS for a) Regional (σ^2=0.43), b) ICA-CSR (σ^2=0.44), and c) GRGS (σ^2=0.6) solutions over 2003-2010. d) GLWD map of surface water over South America. In the dashed blue rectangles, regions of maximum or minimum of TWS signal: 1 – Altiplano, 2 – Solimões-Amazon corridor (including the south of the Amazonian Negro basin) + mouth of the Tocantins, 3 - Pindare and Parnacaiba, 4 – La Plata delta. In the dashed green rectangles, secondary extrema of TWS: 1 – Mouth of the Orinoco, 2 – Sources of Parana (La Plata) and São Francisco rivers, 3 – Patagonia Icefield and Deseado basin.

Figure 3 : a) Temporal component of the 1st PCA mode of TWS for Regional (black), ICA-CSR (red), and GRGS (blue) solutions over 2003-2010. b) Time variations of normalized water levels correlated with the 1st PCA mode: Ciudad Bolivar (black), Serrinha (red), Manaus (blue), Fazenda Vista Alegre (light green), Jatuarana (grey), Obidos (orange), Itaituba (yellow), Porto de Moz (dark green), Batallon 601 (light blue).

Figure 4 : Spatial component of the 2nd PCA mode of TWS for a) Regional (σ^2=0.2), b) ICA-CSR (σ^2=0.15), and c) GRGS (σ^2=0.14) solutions over 2003-2010. d) GLWD map of surface water over South America. In the dashed blue rectangles, regions of maximum or minimum of TWS signal: 1 – Orinoco and the Negro basins, 2 - the southern bank of the Solimões, 3 - the region covered with Pindare and Parnacaiba basins, 4 – the downstream part and the delta of La Plata basin.

Figure 5 : a) Temporal component of the 2nd PCA mode of TWS for Regional (black), ICA-CSR (red), and GRGS (blue) solutions over 2003-2010. b) Time variations of normalized water levels correlated with the 2nd PCA mode: Caracarai (black), Tabatinga (red), Manacapuru (blue), Corrientes (green).

Figure 6 : Spatial component of the 3rd PCA mode of TWS for a) Regional (σ^2=0.13), b) ICA-CSR (σ^2=0.14), and c) GRGS (σ^2=0.1) solutions over 2003-2010. d) GLWD map of surface water over South America. In the dashed blue rectangles, regions of maximum or minimum of TWS signal: 1 – southern bank of the Solimões and the central corridor of the Amazon until the junction with the Tapajos river 2 – upstream part of the Tocantins. In the dashed green rectangles, secondary extrema of TWS: 1 – Negro basin, 2 – Patagonia Icefield and Deseado basin, 3 – Essequibo (Guyana), Suriname (Suriname), Oyapok and Maroni (French Guiana) basins.

Figure 7 : a) Temporal component of the 3rd PCA mode of TWS for Regional (black), ICA-CSR (red), and GRGS (blue) solutions over 2003-2010. b) Time variations of normalized water levels correlated with the 3rd PCA mode: Tucurui (black), Pepiri Mini (red), Chapeton (blue).

Figure 8 : Spatial component of the 4th PCA mode of TWS for a) Regional (σ^2=0.11), b) ICA-CSR (σ^2=0.1), and c) GRGS (σ^2=0.08) solutions over 2003-2010. d) WHYMAP map of groundwater recharge over South America. In the dashed black rectangles, regions of maximum or minimum of TWS signal: 1 – Amazonas, 2 – Maranhão, 3 – Guarani aquifer systems (adapted from Margat (2007)).

Figure 9 : a) Temporal component of the 4th PCA mode of TWS for Regional (black), ICA-CSR (red), and GRGS (blue) solutions over 2003-2010. b) Time variations of normalized water levels correlated with the 4th PCA mode: Piranhas (black), Primera Angostura (red).

Figure 10 : Time-series of GRACE-based TWS over 2003-2010 from Regional (black), ICA CSR 400 km (red), GRGS (blue) expressed in mm of ESL for the a) Amazon, b) Orinoco, c) Tocantins, and d) La Plata basins.

Figure 11 : Time-series of GRACE-based interannual TWS over 2003-2010 from Regional (black), ICA CSR 400 km (red), GRGS (blue) expressed in mm of ESL and of interannual discharge (grey) for the a) Amazon, b) Orinoco, c) Tocantins, and d) La Plata basins.

Table 1 : List of *the in situ* stations used for comparisons with GRACE-derived TWS over the largest river basins South America (Amazon, La Plata, Orinoco, Tocantins, São Francisco, Negro) and their tributaries.

Station	Basin	Lon (°)	Lat (°)	Source
Ciudad Bolivar	Orinoco	-63.608	8.439	HYBAM
Caracarai	Branco (Amazon)	-61.124	1.814	HYBAM
Serrinha	Negro (Amazon)	-64.289	-0.485	HYBAM
Manaus	Negro (Amazon)	-60.035	-3.149	ANA
Tabatinga	Solimões (Amazon)	-69.952	-4.253	HYBAM
Manacapuru	Solimões (Amazon)	-60.609	-3.316	HYBAM
Fazenda Vista Alegre	Madeira (Amazon)	-60.026	-4.898	HYBAM
Jatuarana	Amazon	-59.643	-3.062	ANA
Obidos	Amazon	-55.657	-1.923	HYBAM
Itaituba	Tapajos (Amazon)	-55.982	-4.278	HYBAM
Porto de Moz	Xingu (Amazon)	-52.240	-1.753	ANA
Tucurui	Tocantins	-49.683	-3.783	ANA
Piranhas	São Francisco	-37.756	-9.626	ANA
Corrientes	Parana (La Plata)	-58.833	-27.475	INA
Pepiri Mini	Uruguay (La Plata)	-53.933	-27.154	INA
Batallon 601	Coronda (La Plata)	-60.746	-31.694	INA
Chapeton	Parana (La Plata)	-60.283	-31.574	INA
Primera Angostura	Negro	-63.790	-40.456	INA

Table 2 : Explained variances for the four first modes of the Principal Components Analysis (PCA) of centred and deseasonalized TWS from GRACE for the regional solutions, the ICA-filtered solutions from CSR, GFZ, and JPL, and the GRGS solutions over the 2003-2010 time-period.

Explained variance (%)	mode 1	mode 2	mode 3	mode 4	sum
regional	43	20	13	11	87
ICA CSR	44	15	14	10	83
ICA GFZ	42	17	13	10	82
ICA JPL	41	21	13	8	83
GRGS	60	14	10	8	92

Table 3 : Correlation between the spatial component of the different GRACE solutions (regional, ICA-CSR-400km, and GRGS) for each PCA mode.

R	GRACE solutions		
PCA mode	regional vs. ICA-CSR-400km	regional vs. GRGS	ICA-CSR-400km vs. GRGS
mode 1	0.84	0.6	0.67
mode 2	0.67	0.43	-0.04
mode 3	0.69	0.46	0.38
mode 4	0.46	0.86	0.39

Table 4 : Correlation between the temporal component of the different GRACE solutions (regional, ICA-CSR-400km, and GRGS), and maximum correlation and associated time-lag for each PCA mode.

R		GRACE solutions		
PCA mode		regional vs. ICA-CSR-400km	regional vs. GRGS	ICA-CSR-400km vs. GRGS
mode 1	R(Δt=0)	0.95	0.82	0.81
	Rmax (Δt in days)	0.96 (30)	0.84 (80)	0.86 (180)
mode 2	R(Δt=0)	0.79	0.52	0.08
	Rmax (Δt in days)	0.91 (-120)	0.80 (-160)	0.58 (-180)
mode 3	R(Δt=0)	0.79	0.56	0.17
	Rmax (Δt in days)	0.79 (0)	0.61 (-60)	0.21 (60)
mode 4	R(Δt=0)	0.62	0.96	0.47
	Rmax (Δt in days)	0.7 (-120)	0.96 (0)	0.57 (180)

Table 5 : Correlation value corresponding to maximum of module of correlation and associated time-lag (days) between interannual variations of *in situ* water levels and GRACE-based TWS for regional, ICA (CSR), and GRGS solutions.

		regional		ICA		GRGS	
Station	PCA Mode	R max(|R|)	Δt (days)	R max(|R|)	Δt (days)	R max(|R|)	Δt (days)
Ciudad Bolivar	1	-0.80	180	-0.73	180	-0.63	170
Caracarai	2	-0.86	-40	-0.83	30	-0.66	-120
Serrinha	1	0.66	-160	0.62	-150	0.62	-180
Manaus	1	0.65	120	0.65	60	0.50	-180
Tabatinga	2	0.81	-160	0.83	-90	0.39	-180
Manacapuru	2	0.91	-180	0.83	-90	0.47	-180
Fazenda Vista Alegre	1	0.80	50	0.84	90	0.75	-160
Jatuarana	1	0.70	30	0.70	60	0.58	-180
Obidos	1	0.88	-20	0.87	30	0.81	-120
Itaituba	1	0.96	0	0.83	-110	0.94	30
Porto de Moz	1	0.88	-90	0.82	0	0.71	-160
Tucurui	3	0.74	-30	0.73	30	0.31	-30
Piranhas	4	0.68	-30	0.71	-30	0.71	-30
Pepiri Mini	3	-0.70	-150	-0.80	-120	-0.16	-180
Corrientes	2	0.71	70	0.52	60	0.90	-100
Batallón 601	1	-0.67	-110	-0.62	-90	0.25	180
Chapeton	3	-0.77	-160	-0.72	-150	-0.39	-180
Primera Angostura	4	-0.70	-150	-0.52	180	-0.77	-150

Table 6 : Maximum correlation and associated time-lag (months) between interannual variations of GRACE-based TWS (expressed in ESL) for regional, ICA (CSR), and GRGS solutions of *in situ* river discharge in Obidos – Amazon, Ciudad Bolivar – Orinoco, Tucurui – Tocantins, and Chapeton – La Plata.

	TWS regional		TWS ICA		TWS GRGS	
Discharge station	Rmax	Δt (months)	Rmax	Δt (months)	Rmax	Δt (months)
Obidos (Amazon)	0.9	1	0.93	1	0.92	1
Ciudad Bolivar (Orinoco)	0.69	-1	0.58	-1	0.69	-2
Tucurui (Tocantins)	0.46	2	0.63	1	0.37	2
Chapeton (La Plata)	0.86	-3	0.61	-3	0.75	-3

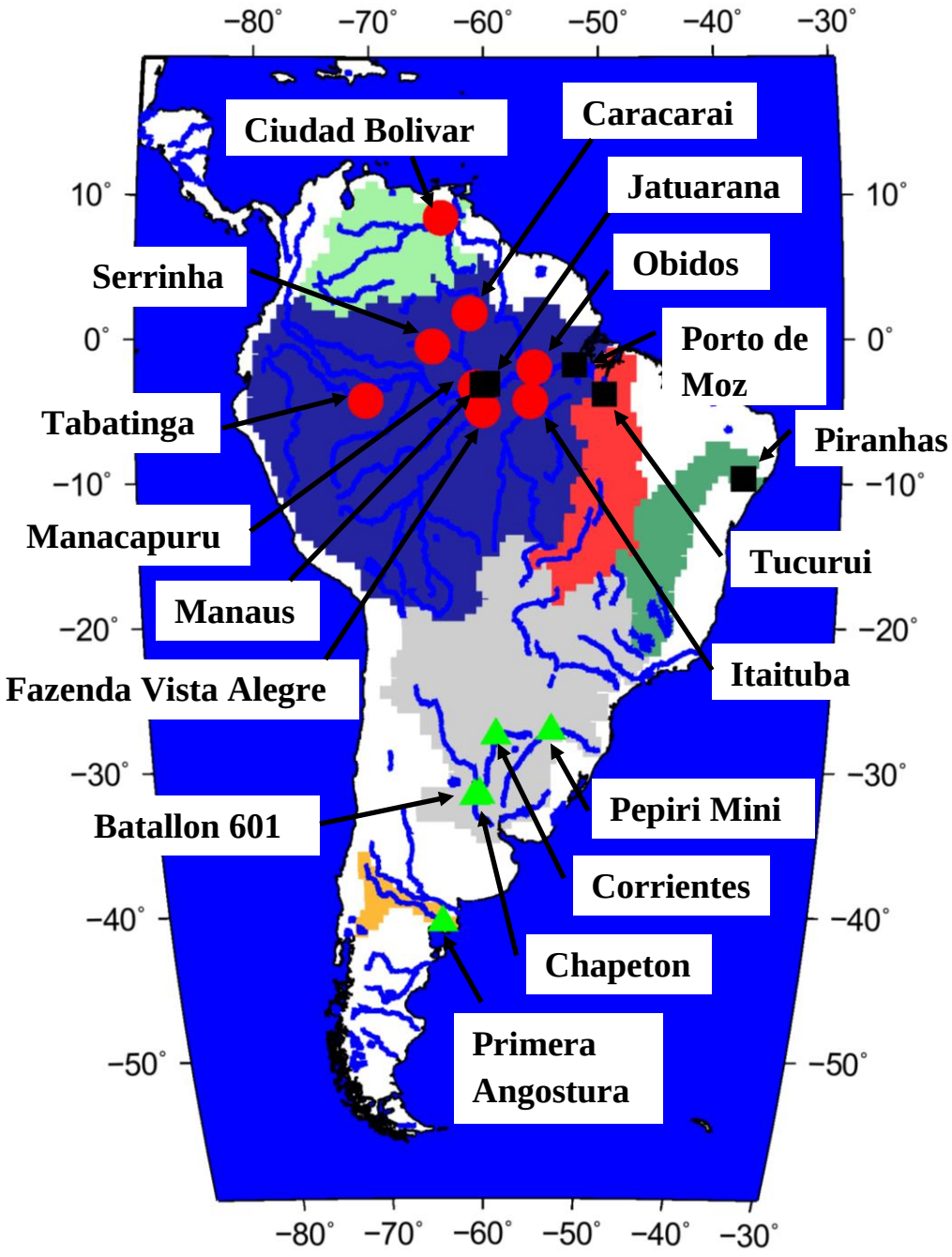

Figure 1 : Major drainage basins of South America: Orinoco (light green), Amazon (dark blue), Tocantins (red), São Francisco (dark green), La Plata (grey), Negro (orange). *In situ* gauge stations are represented with red circles (HYBAM), black squares (ANA), and green triangles (INA).

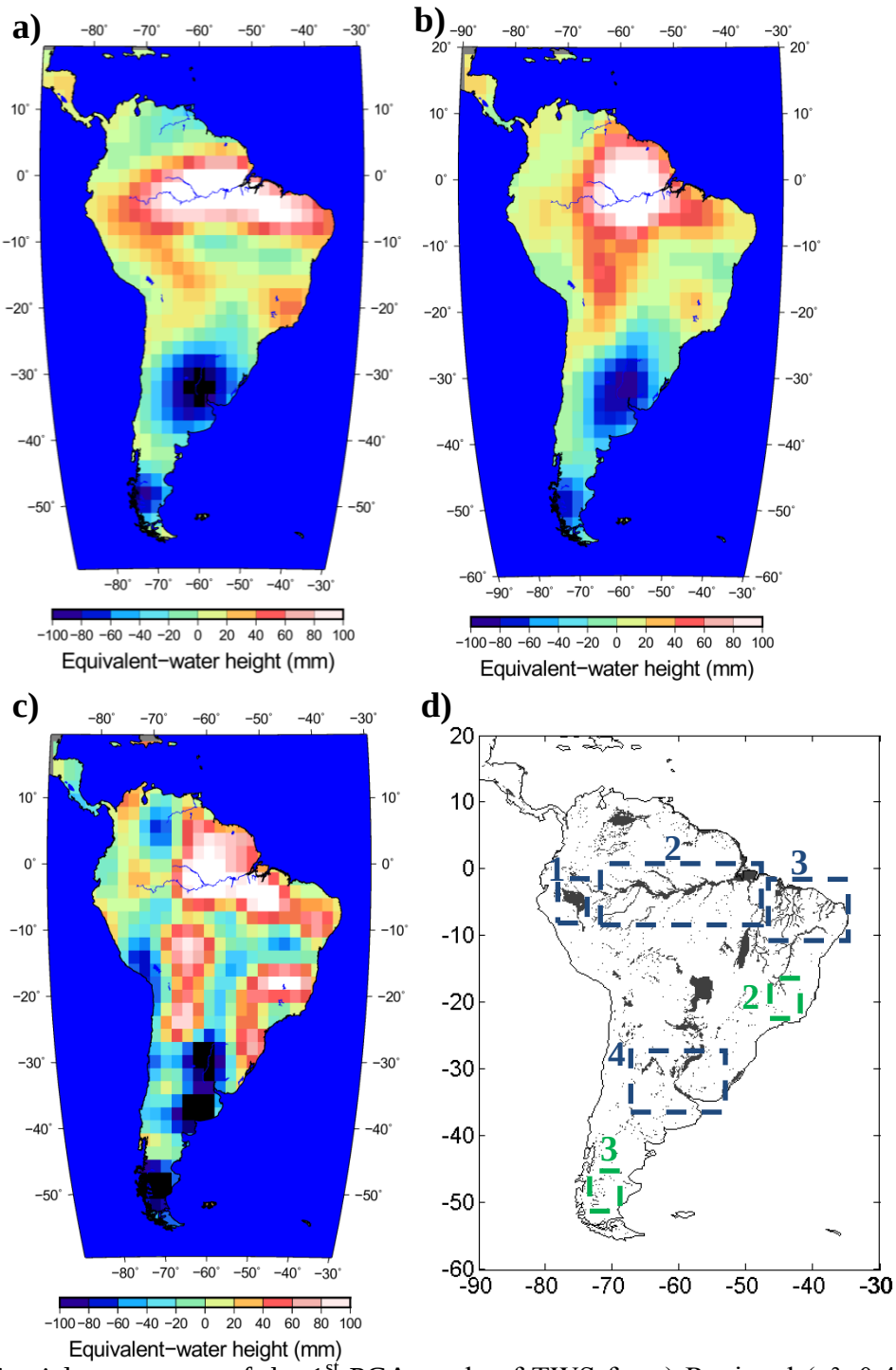

Figure 2 : Spatial component of the 1st PCA mode of TWS for a) Regional (σ^2=0.43), b) ICA-CSR (σ^2=0.44), and c) GRGS (σ^2=0.6) solutions over 2003-2010. d) GLWD map of surface water over South America. In the dashed blue rectangles, regions of maximum or minimum of TWS signal: 1 – Altiplano, 2 – Solimões-Amazon corridor (including the south of the Amazonian Negro basin) + mouth of the Tocantins, 3 - Pindare and Parnacaiba, 4 – La Plata delta. In the dashed green rectangles, secondary extrema of TWS: 1 – Mouth of the Orinoco, 2 – Sources of Parana (La Plata) and São Francisco rivers, 3 – Patagonia Icefield and Deseado basin.

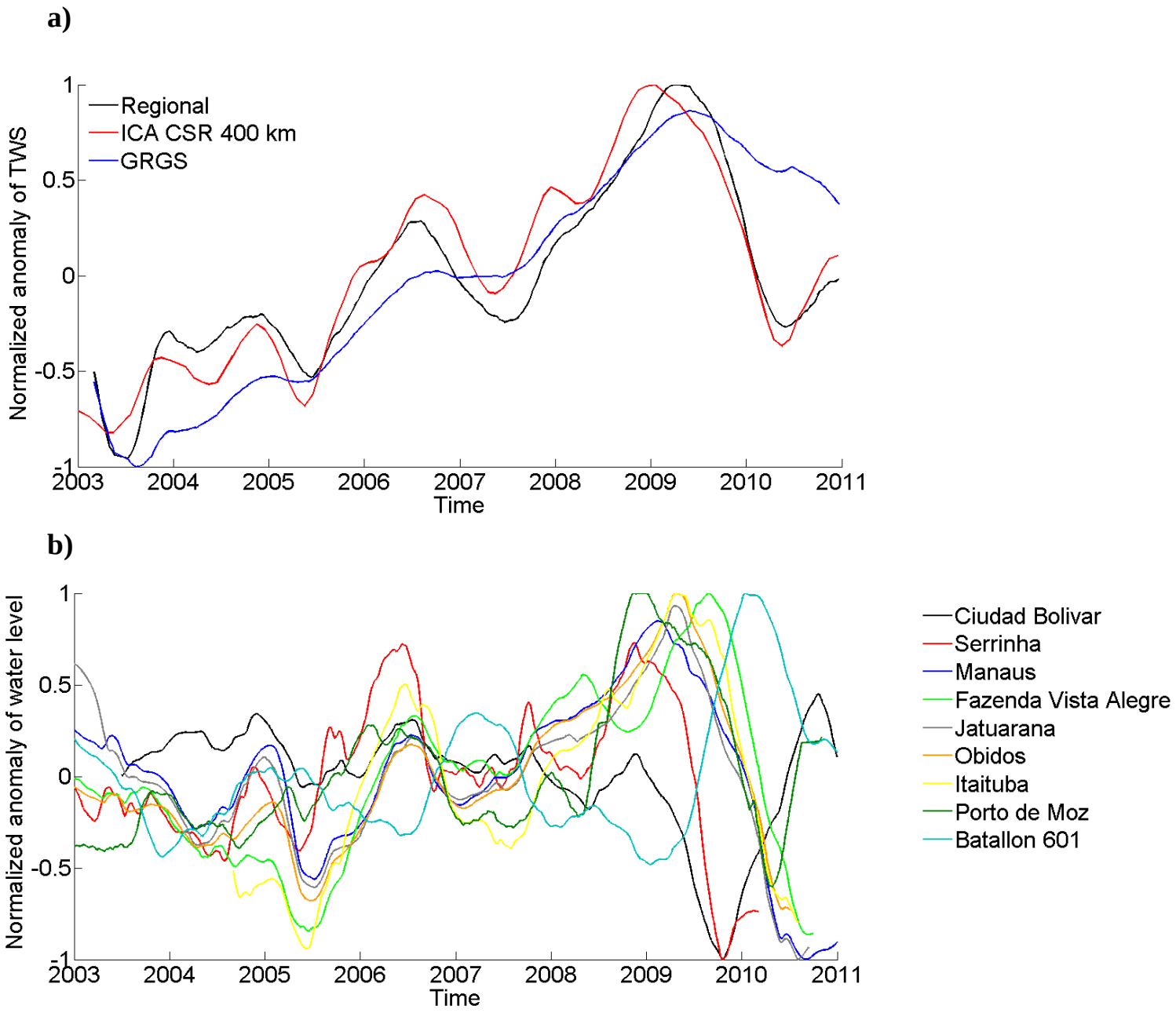

Figure 3 : a) Temporal component of the 1st PCA mode of TWS for Regional (black), ICA-CSR (red), and GRGS (blue) solutions over 2003-2010. b) Time variations of normalized water levels correlated with the 1st PCA mode: Ciudad Bolivar (black), Serrinha (red), Manaus (blue), Fazenda Vista Alegre (light green), Jatuarana (grey), Obidos (orange), Itaituba (yellow), Porto de Moz (dark green), Batallon 601 (light blue).

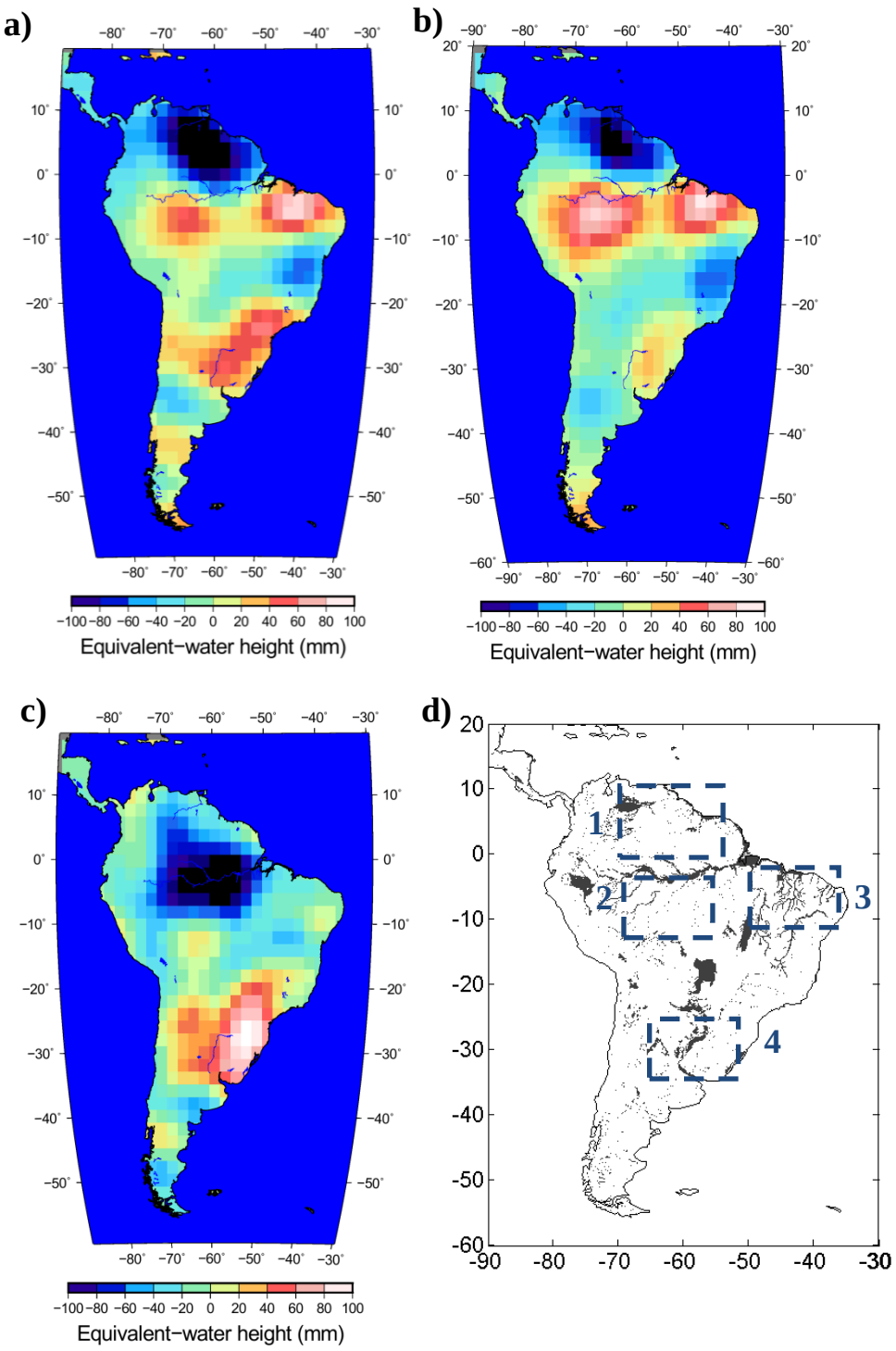

Figure 4 : Spatial component of the 2nd PCA mode of TWS for a) Regional (σ^2=0.2), b) ICA-CSR (σ^2=0.15), and c) GRGS (σ^2=0.14) solutions over 2003-2010. d) GLWD map of surface water over South America. In the dashed blue rectangles, regions of maximum or minimum of TWS signal: 1 – Orinoco and the Negro basins, 2 - the southern bank of the Solimões, 3 - the region covered with Pindare and Parnacaiba basins, 4 – the downstream part and the delta of La Plata basin.

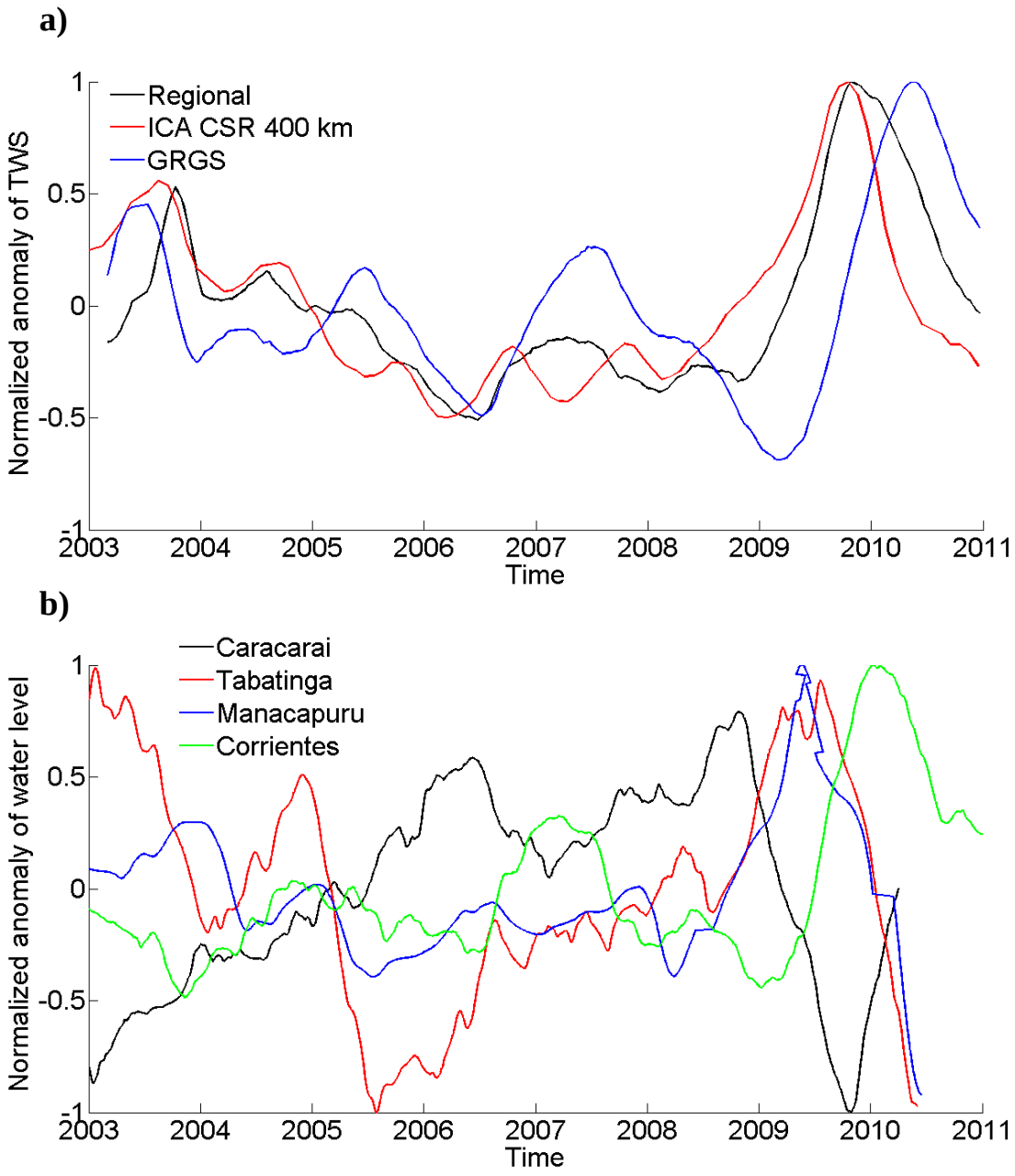

Figure 5 : a) Temporal component of the 2nd PCA mode of TWS for Regional (black), ICA-CSR (red), and GRGS (blue) solutions over 2003-2010. b) Time variations of normalized water levels correlated with the 2nd PCA mode: Caracarai (black), Tabatinga (red), Manacapuru (blue), Corrientes (green).

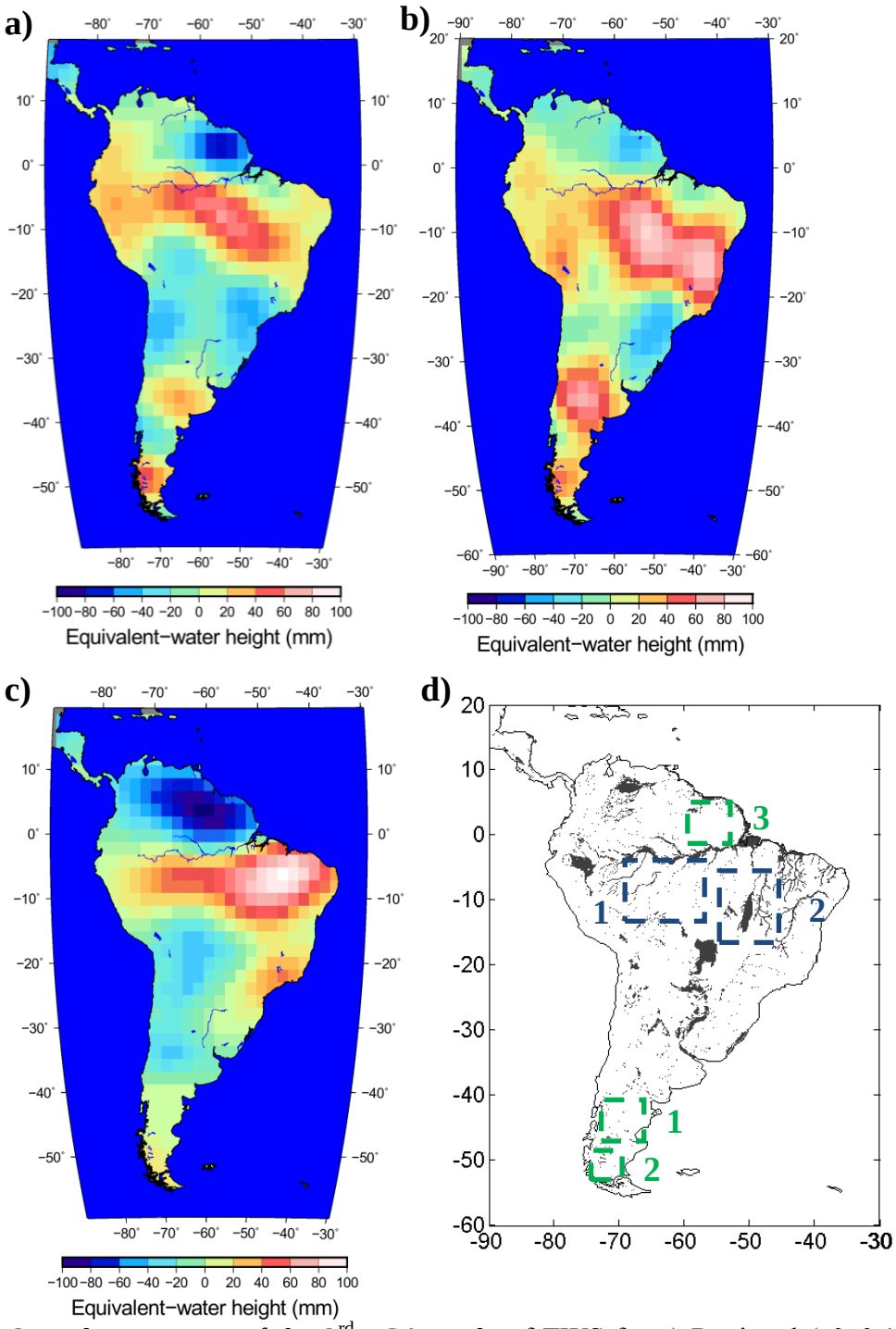

Figure 6 : Spatial component of the 3rd PCA mode of TWS for a) Regional (σ^2=0.13), b) ICA-CSR (σ^2=0.14), and c) GRGS (σ^2=0.1) solutions over 2003-2010. d) GLWD map of surface water over South America. In the dashed blue rectangles, regions of maximum or minimum of TWS signal: 1 – southern bank of the Solimões and the central corridor of the Amazon until the junction with the Tapajos river 2 – upstream part of the Tocantins. In the dashed green rectangles, secondary extrema of TWS: 1 – Negro basin, 2 – Patagonia Icefield and Deseado basin, 3 – Essequibo (Guyana), Suriname (Suriname), Oyapok and Maroni (French Guiana) basins.

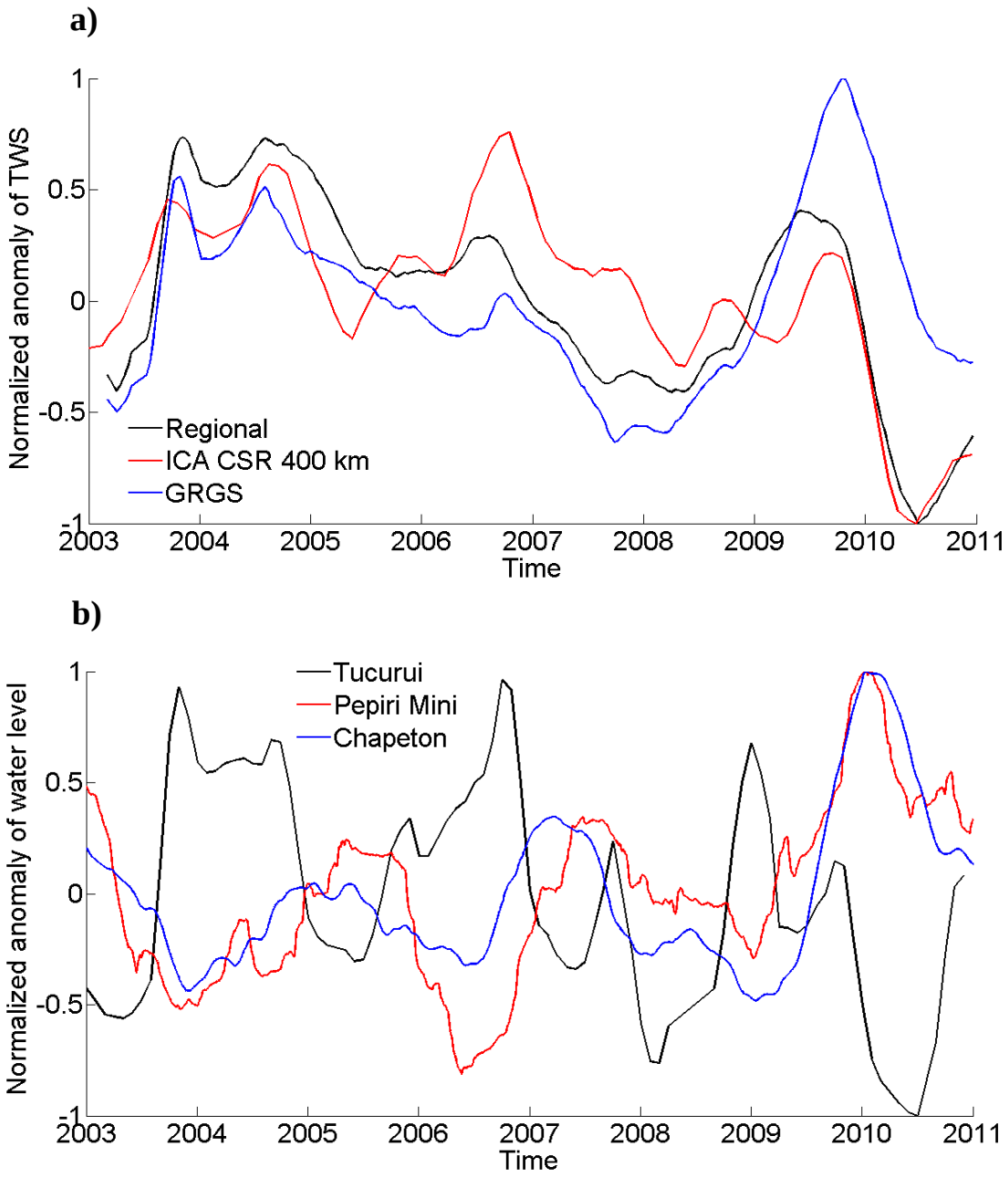

Figure 7 : a) Temporal component of the 3rd PCA mode of TWS for Regional (black), ICA-CSR (red), and GRGS (blue) solutions over 2003-2010. b) Time variations of normalized water levels correlated with the 3rd PCA mode: Tucurui (black), Pepiri Mini (red), Chapeton (blue).

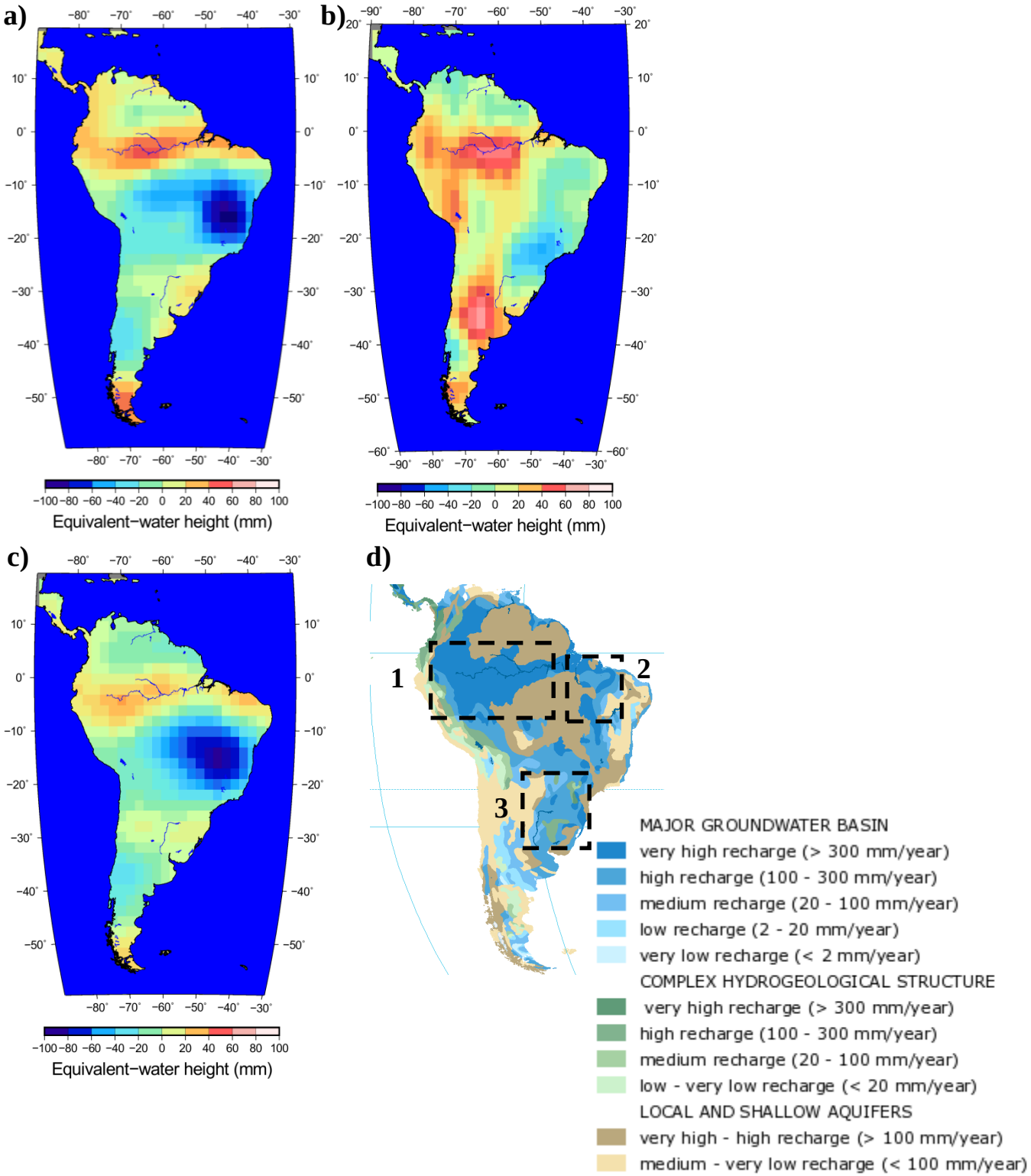

Figure 8 : Spatial component of the 4th PCA mode of TWS for a) Regional (σ^2=0.11), b) ICA-CSR (σ^2=0.1), and c) GRGS (σ^2=0.08) solutions over 2003-2010. d) WHYMAP map of groundwater recharge over South America. In the dashed black rectangles, regions of maximum or minimum of TWS signal: 1 – Amazonas, 2 – Maranhão, 3 – Guarani aquifer systems (adapted from Margat (2007)).

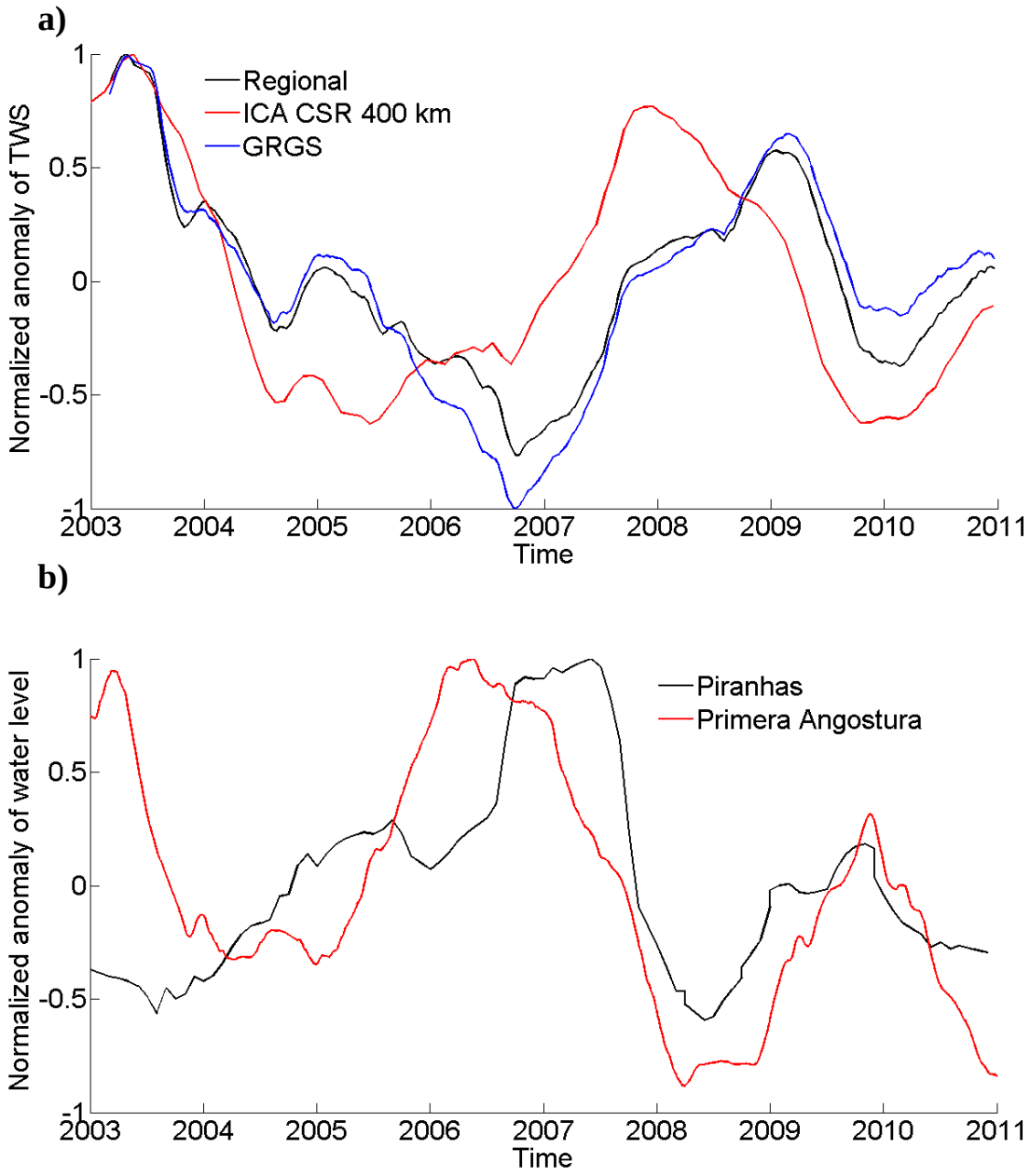

Figure 9 : a) Temporal component of the 4th PCA mode of TWS for Regional (black), ICA-CSR (red), and GRGS (blue) solutions over 2003-2010. b) Time variations of normalized water levels correlated with the 4th PCA mode: Piranhas (black), Primera Angostura (red).

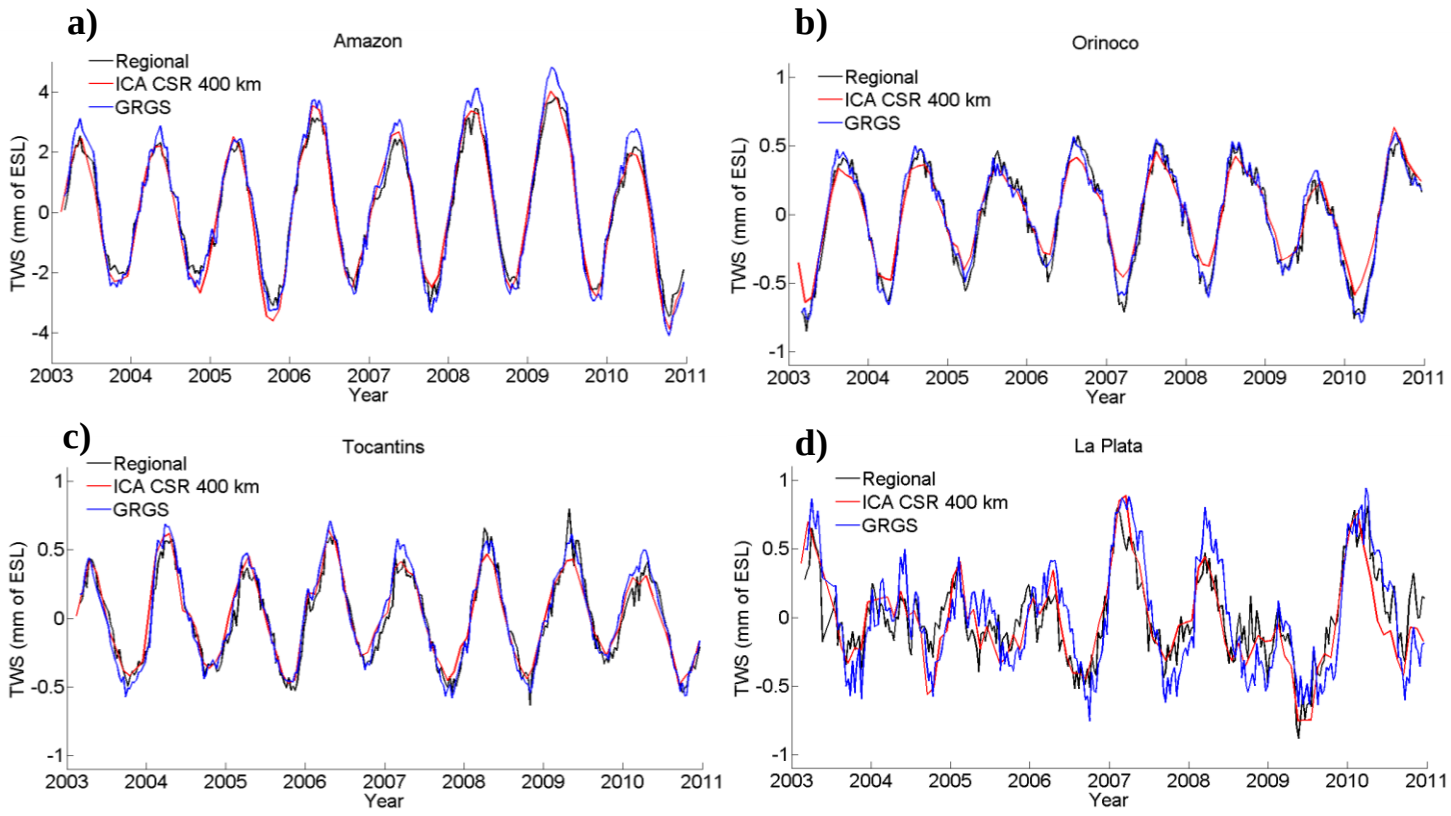

Figure 10 : Time-series of GRACE-based TWS over 2003-2010 from Regional (black), ICA CSR 400 km (red), GRGS (blue) expressed in mm of ESL for the a) Amazon, b) Orinoco, c) Tocantins, and d) La Plata basins.

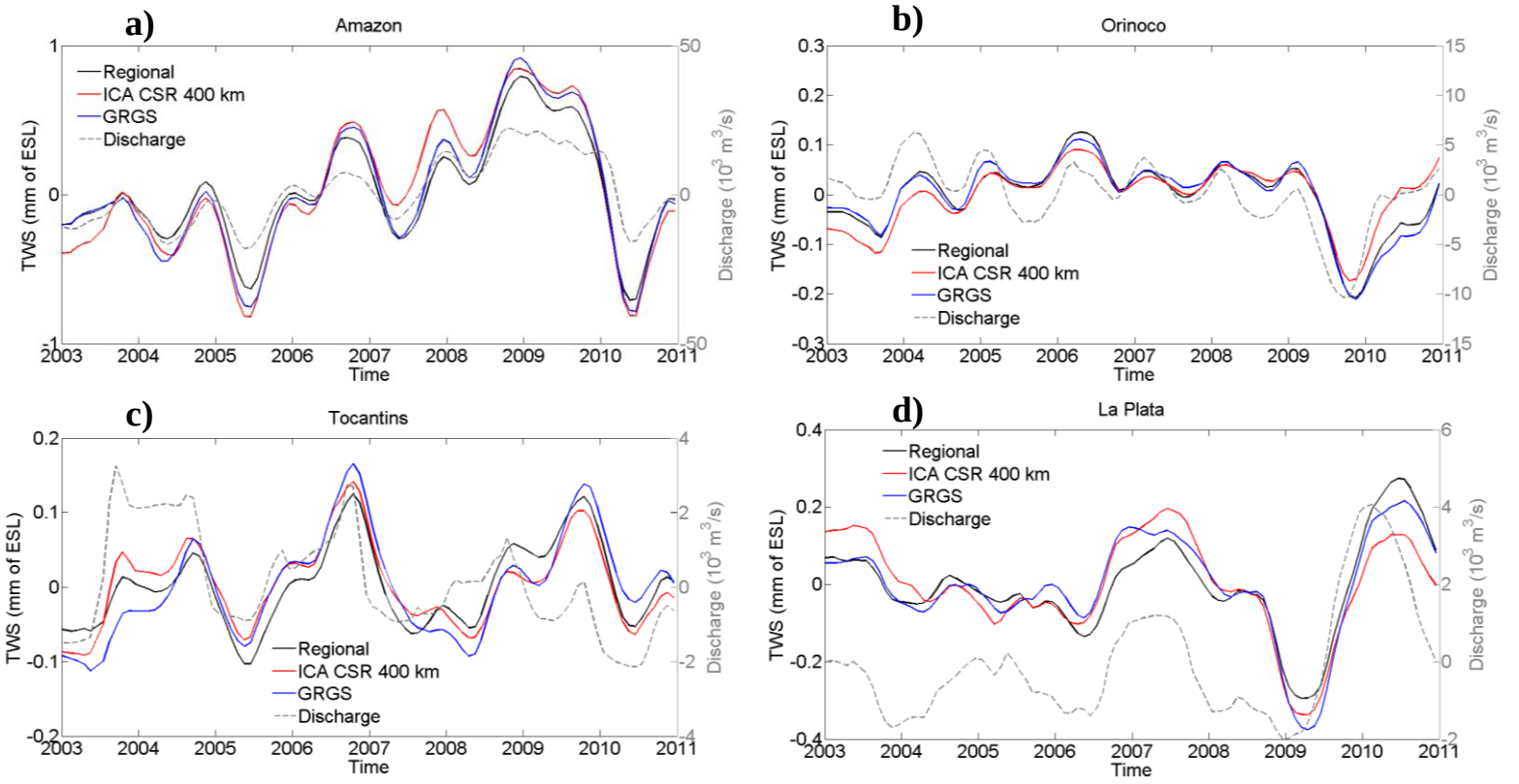

Figure 11 : Time-series of GRACE-based interannual TWS over 2003-2010 from Regional (black), ICA CSR 400 km (red), GRGS (blue) expressed in mm of ESL and of interannual discharge (grey) for the a) Amazon, b) Orinoco, c) Tocantins, and d) La Plata basins.